Check for updates

Clinical Science (2021) **135** 2285–2305
https://doi.org/10.1042/CS20210183

PORTLAND PRESS

Research Article

Selective HIF stabilization alleviates hepatocellular steatosis and ballooning in a rodent model of 70% liver resection

Samuele Iesari[1,2,3,4], Isabelle Leclercq[5], Nicolas Joudiou[6], Mina Komuta[7], Aurélie Daumerie[8], Jérôme Ambroise[9], Alexandra Dili[5], Natacha Feza-Bingi[5], Daela Xhema[1], Caroline Bouzin[8], Bernard Gallez[6], Francesco Pisani[2], Eliano Bonaccorsi-Riani[1,3] and Pierre Gianello[1]

[1]Pôle de Chirurgie Expérimentale et Transplantation, Institut de Recherche Expérimentale et Clinique, Université catholique de Louvain, Brussels, Belgium; [2]Department of Biotechnological and Applied Clinical Sciences, University of L'Aquila, L'Aquila, Italy; [3]Liver Transplantation, Service de Chirurgie Générale et Transplantation Abdominale, Cliniques Universitaires Saint-Luc, Brussels, Belgium; [4]Kidney Transplantation, Fondazione IRCCS Ca' Granda Ospedale Maggiore Policlinico, Milan, Italy; [5]Laboratory of Hepato-Gastroenterology, Institut de Recherche Expérimentale et Clinique, Université catholique de Louvain, Brussels, Belgium; [6]Nuclear and Electron Spin Technologies, Louvain Drug Research Institute, Université catholique de Louvain, Brussels, Belgium; [7]Department of Pathology, Keio University, Tokyo, Japan; [8]IREC Imaging Platform, Institut de Recherche Expérimentale et Clinique, Université catholique de Louvain, Brussels, Belgium; [9]Centre for Applied Molecular Technologies, Institut de Recherche Expérimentale et Clinique, Université catholique de Louvain, Brussels, Belgium

Correspondence: Samuele Iesari (samuele.iesari@uclouvain.be)

Background: Small-for-size syndrome (SFSS) looms over patients needing liver resection or living-donor transplantation. Hypoxia has been shown to be crucial for the successful outcome of liver resection in the very early postoperative phase. While poorly acceptable as such in real-world clinical practice, hypoxia responses can still be simulated by pharmacologically raising levels of its transducers, the hypoxia-inducible factors (HIFs).
We aimed to assess the potential role of a selective inhibitor of HIF degradation in 70% hepatectomy (70%Hx).
Methods: In a pilot study, we tested the required dose of roxadustat to stabilize liver HIF1α. We then performed 70%Hx in 8-week-old male Lewis rats and administered 25 mg/kg of roxadustat (RXD25) at the end of the procedure. Regeneration was assessed: ki67 and 5-ethynyl-2′-deoxyuridine (EdU) immunofluorescent labeling, and histological parameters. We also assessed liver function via a blood panel and functional gadoxetate-enhanced magnetic resonance imaging (MRI), up to 47 h after the procedure. Metabolic results were analyzed by means of RNA sequencing (RNAseq).
Results: Roxadustat effectively increased early HIF1α transactivity. Liver function did not appear to be improved nor liver regeneration to be accelerated by the experimental compound. However, treated livers showed a mitigation in hepatocellular steatosis and ballooning, known markers of cellular stress after liver resection. RNAseq confirmed that roxadustat unexpectedly increases lipid breakdown and cellular respiration.
Conclusions: Selective HIF stabilization did not result in an enhanced liver function after standard liver resection, but it induced interesting metabolic changes that are worth studying for their possible role in extended liver resections and fatty liver diseases.

Received: 17 February 2021
Revised: 21 September 2021
Accepted: 22 September 2021

Accepted Manuscript online: 22 September 2021
Version of Record published: 13 October 2021

Introduction

In liver surgery, the management of liver resection in cirrhotic patients or small-size hepatic remnants even in healthy livers still represents a challenge. The postoperative conundrum alternatively called post-hepatectomy liver failure (PHLF) or small-for-size syndrome (SFSS) is the major cause of death after liver resection [1].

© 2021 The Author(s). Published by Portland Press Limited on behalf of the Biochemical Society

Downloaded from http://portlandpress.com/clinsci/article-pdf/135/19/2285/921840/cs-2021-0183.pdf by Universita degli Studi di Milano user on 18 October 2021

Clinical Science (2021) **135** 2285–2305
https://doi.org/10.1042/CS20210183

In recent years, selective liver hypoxia has been shown to be beneficial after extended hepatectomy. In rat models of human associating liver partition and portal vein ligation technique for two-stage hepatectomy (ALPPS), parenchymal hypoxia, resulting from a reduced arterial flow, has been associated with accelerated liver regeneration after portal vein ligation and parenchymal transection [2], and evidence showed that ALPPS curbs mortality after extended liver resection [3,4]. Indeed, post-hepatectomy hypoxia-driven response induces new vessels formation and reduces the shift between hepatocellular and vessel proliferation by slowing down the former and accelerating the latter [4,5]. Tissue hypoxia activates the α subunits of hypoxia-inducible factor (HIF) transcription factors, HIF1α and HIF2α, which mediate a wide array of responses to parenchymal low oxygen pressure. Accordingly, increased HIF-α transactivity leads to new blood vessel formation in response to hypoxic injury [6]. In view of the translational relevance of these findings, introducing hypoxia in hepatobiliary surgery is an appealing perspective, though apparently unrealistic because it is known that systemic hypoxia impairs hepatic regeneration [7], and that the human biliary tract is exquisitely sensitive to hypoxia [8]. The inhibition of prolyl hydroxylase domain (PHD) proteins effectively increases HIF-α activity. PHDs require oxygen, iron, and α-ketoglutarate, to hydroxylate HIFs and steer them towards degradation. In this regard, PHDs are considered intracellular oxygen sensors. Several molecules inhibit PHD function, such as deferoxamine, dimethyloxalylglycine (DMOG), ethyl-3,4-dihydroxybenzoate (EDHB), and selective PHD inhibitors [6,9–11]. Indeed, deferoxamine protects from oxidative stress and ischemia/reperfusion injury (IRI) in animal models of liver resection [12–19]. DMOG increases sinusoidal endothelium density [11], preserves sinusoidal diameter, and significantly improves survival after 87% hepatectomy in rats [4]. EDHB acts as a preconditioning agent and improves liver regeneration after ALPPS-like procedure, by inducing cell cycle-promoting cyclins [9]. Because of their mechanism of action, the cited PHD inhibitors lack selectivity [20]. DMOG and EDHB compete with ketoglutaric acid and inhibit other α-ketoglutarate-dependent dioxygenases [21,22]. Deferoxamine sequesters iron, which is required for PHD activity, but it affects any iron-requiring enzymes. Recently, a new class of selective PHD inhibitors has been released: the isoquinolines, collectively known as HIF stabilizers because they selectively compete for the active site of PHDs. Among them, roxadustat (FibroGen, San Francisco, CA, U.S.A.), a small (352.34 Da) orally active molecule, appears particularly promising and has been already licensed in the European Union and China to treat anemia in end-stage renal disease as erythropoietin release is controlled by HIF-α [23,24]. Besides, the effects of this entire class of molecules have not yet been reported in the framework of liver resection. Roxadustat reported half-life in Sprague–Dawley rats is 3.4–5.6 h and is not dose-dependent. To obtain a steady hematocrit increase, it is chronically administered to rats three times a week [25]. Chronic administration of roxadustat > 15 mg/kg yields polycythemia and associated adverse events in rats, while doses up to 10 mg/kg are active and do not induce significant mortality [25–27]. The intraperitoneal injection of roxadustat is known to effectively target the liver and stabilize HIF-α with a peak at 6 h after administration in mice [24], while residual HIF1α stabilization is detectable after 30 h in an *ex-situ* liver graft perfusion model [26].

Thus, we hypothesized that the beneficial effects elicited by hypoxia after liver resection are linked to HIF-associated response pathways. We chose a standard rat model of 70% hepatectomy (70%Hx), known to induce intense liver regeneration without mortality [28]. We aimed to assess whether a selective pharmacological HIF stabilization, obtained by the administration of roxadustat, affects liver function and regeneration postoperatively.

Methods

Animals

Male Lewis rats came from Janvier Labs (Le Genest-Saint-Isle, France). At the time of the procedure, they were 8 weeks old and weighed 244 g (interquartile range, IQR = 234–247). The animals had been housed for at least 6 days in the local animal facility (Laboratory of Experimental Surgery and Transplantation, Harvey Tower, 4th floor, 55 Avenue Hippocrate, 1200 Brussels, Belgium) before the experimental procedures, which took place in the same laboratory. The animals were kept in standard cages, in 12-h light–dark cycle, and received standard chow and drinking water *ad libitum*. Our institutional review board approved this protocol number 2019/UCL/MD/043 on 17 December 2019.

Pharmacological pilot study

Dosage, timing of injection, and effectiveness of intraperitoneally administered roxadustat in inducing liver HIF stabilization was assessed through a pharmacological study that entailed three groups of three rats each: the first receiving roxadustat 10 mg/kg (the RXD10 group), the second receiving RXD 25 mg/kg (the RXD25 group), and the third undergoing hepatic artery ligature at the hilum (the HAL group). Animals were euthanized at three time points: baseline, 60 min, and 6 h. Toxicity was assessed via a biochemical panel and death rate. Effectiveness was assessed through HIF1α measurement in cytosolic and nuclear liver extracts, and the evaluation of expression of HIF-regulated genes.

Downloaded from http://portlandpress.com/clinsci/article-pdf/135/19/2285/921840/cs-2021-0183.pdf by Universita degli Studi di Milano user on 18 October 2021

© 2021 The Author(s). Published by Portland Press Limited on behalf of the Biochemical Society

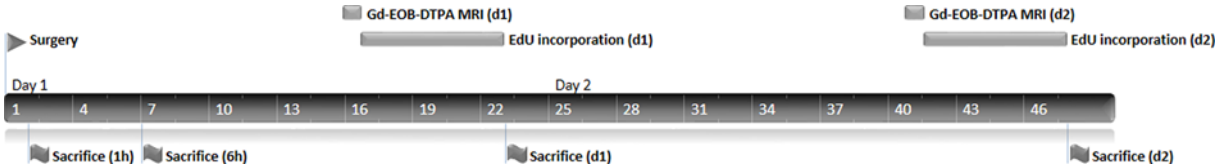


Figure 1. Timeline

Surgery

General anesthesia was obtained with isoflurane in oxygen at 2 l/min: induction 4%, maintenance 2% (IsoFlo, Zoetis, Parsippany, NJ, U.S.A.). Pre- and post-operative analgesia entailed subcutaneously injected buprenorphine 0.01 mg/kg (Temgesic, Schering-Plough, Kenilworth, NJ, U.S.A.), and ketoprofen 2 mg/kg (Ketofen, Zoetis).

70%Hx was performed by removing the median and the left lateral lobes after median laparotomy, according to the principles described by Higgins and Anderson [29]. Since the ligation at the basis of the median lobe might constrict the lumen of the inferior vena cava, we ligated the vascular pedicles individually, we divided the median lobe into its right and left segments, finally the lobes were ligated and severed one by one, according to Kubota et al. [30].

In the sham procedure, rats underwent median laparotomy and dissection of liver ligaments. The liver was wrapped in humid gauze for the duration of the procedure.

All the procedures were carried out during the afternoon (between 3:30 p.m. and 10:00 p.m.) to ensure that animals had a spontaneously empty foregut.

Study groups and postoperative follow-up

At the end of surgery, a single intraperitoneal dose of roxadustat 25 mg/kg was injected. The drug was dissolved in dimethyl sulfoxide (DMSO, Sigma–Aldrich, St. Louis, MO, U.S.A.) and then diluted in pH 7.4 phosphate-buffered saline (PBS) to a 2% concentration of DMSO. The placebo consisted of 2% DMSO-PBS, in the same volume as the experimental drug. Postoperatively, all rats received a single subcutaneous shot of 4 ml/kg of 2.1% $NaHCO_3$ and had free access to food and 20% glucose as drinking water to avoid post-resection hypoglycemia [28].

Our study included three groups of animals (hepatectomy and roxadustat [70%Hx-RXD25], hepatectomy and placebo [70%Hx-placebo], and sham procedure and placebo [sham-placebo]), which underwent blood sampling and euthanasia after 1 (1 h), 6 (6 h), 22 (day 1, d1), and 47 h (day 2, d2) from the end of surgery and drug administration. At 15 and 40 h after surgery, rats whose euthanasia was planned on d1 and d2 underwent contrast-enhanced magnetic resonance imaging (MRI). The animals then received an intraperitoneal injection of 50 mg/kg of 5-ethynyl-2′-deoxyuridine (EdU, Carbosynth, Compton, U.K.) and were euthanized 6 h later (Figure 1).

Tissue assays

Liver nuclear and cytosolic protein extracts were obtained with the Nuclear Extract Kit (#40010, Active Motif, Carlsbad, CA, U.S.A.) and concentrations were measured via a bicinchoninic acid assay. HIF-1α and -2α were quantified in subcellular extracts using an enzyme-linked immunosorbent assay (#LS-F11633 and #LS-F9117, LSBio, Seattle, WA, U.S.A.), as per manufacturer's instructions. Total liver lipids were extracted with water, methanol, and chloroform, and quantified by the vanillin-phosphoric acid reaction.

Assessment of the hepatic function with MRI

MRI experiments were performed on a Bruker Biospec 11.7 Tesla (Bruker Biospin GmbH, Ettlingen, Germany) equipped with a volume coil (inner diameter; 74 mm). Animals were anesthetized during imaging session with isoflurane mixed with air at 3.5% for induction and 2% for maintenance (duration approx. 1 h). Estimation of global hepatocellular function was obtained through gadolinium ethoxybenzyl diethylenetriamine pentaacetic acid (Gd-EOB-DTPA, Primovist, Bayer, Leverkusen, Germany)-enhanced MRI using a dynamic contrast-enhanced sequence [31,32]. The contrast agent was injected intravenously via a catheter in the tail vein, at a dose of 0.025 mmol/kg for 30 s after the beginning of the acquisition [33–35]. Acquisition parameters were as follows: TE: 1.2 ms, TR: 9.62 ms, NA: 3, number of repetitions: 500, TA: 33 min, FA: 15°, FOV: 60 × 60 mm^2, Mat: 128 × 128, slice thickness: 1 mm. The resulting temporal resolution was 4 s. In post-processing, we selected the regions of interest (ROIs) in the right lobe from which we averaged the signal. The hepatic function was estimated with a homemade algorithm on Matlab (MathWorks, Natick, MA, U.S.A.) by fitting the signal from the ROI [36]. We obtained the following parameters from the curve: time to peak, i.e. the delay between the arrival time (t_0) of the contrast agent and the maximum signal in

Downloaded from http://portlandpress.com/clinsci/article-pdf/135/19/2285/921840/cs-2021-0183.pdf by Universita degli Studi di Milano user on 18 October 2021

© 2021 The Author(s). Published by Portland Press Limited on behalf of the Biochemical Society

Clinical Science (2021) **135** 2285–2305
https://doi.org/10.1042/CS20210183

the ROI, time to 30% signal decay, i.e. the delay between the maximum signal and its reduction in 30%, and the areas under the curve (AUC) between t_0 and t_0+60 s (AUC60), and between t_0 and t_0+90 s (AUC90) [37]. We calculated the AUC between t_0 and the time to peak and the whole AUC.

Biochemistry

Complete blood cell count was done with the MS-9/3 (Melet Schloesing, La Chaux-de-Fonds, Switzerland). Lactate and pH were measured with the i-STAT (Abbot, Chicago, IL, U.S.A.). Serum analytes were measured with the DRI-CHEM NX500i (Fujifilm, Tokyo, Japan): albumin, bilirubin, NH_3, AST, ALT, creatinine. Plasma factor V was measured via an enzyme-linked immunosorbent assay (ELISA, #DL-F5-Ra, DlDevelop, Jiangsu, China). Peripheral and portal plasma triglycerides, total cholesterol, and HDL were measured with the DRI-CHEM NX500i (Fujifilm, Tokyo, Japan). Plasma erythropoietin levels were measured with the rat erythropoietin ELISA Kit, #E-EL-R0007 (Elabscience, Houston, TX, U.S.A.) following the manufacturer's instructions.

Histology

An experienced liver pathologist evaluated Hematoxylin–Eosin (H&E)-stained whole-liver sections following these parameters: presence of mitoses, inflammation, endothelial denudation, microvascular thrombosis, parenchymal hemorrhage, hepatocellular ballooning, steatosis, and necrosis. Endothelial denudation was defined as enlargement of endothelial nuclei or endothelial dislocation or extravasation of red blood cells in the Disse space. Hepatocellular ballooning was defined as clear-cell change with doubling in size of hepatocytes. Steatosis was further classified based on its location [38], its proportion ($<$5, 5–33, 33–66, $>$66%), and the type of lipid droplets (micro- or macrovesicular). Steatosis involving $\geq$5% of hepatocytes was considered relevant.

Fluorescence immunostaining, whole-slide imaging, and quantitative evaluation of immunostaining

Paraffin-embedded sections were deparaffinized. Endogenous peroxidases were inhibited with 3% hydrogen peroxide in methanol for 20 min. Antigens were retrieved in pH 5.7 10 mM citrate buffer. Aspecific antigen binding sites were blocked in tris-buffered saline (TBS) + 5% bovine serum albumine + 0.1% Tween20. Slides were then submitted to Ki67 staining or EdU revelation. Anti-Ki67 primary antibody (rabbit, clone SP6, #ab16667, 1/100 dilution, Abcam, Cambridge, U.K.) was incubated for 90 min at room temperature (RT). Slides were then incubated with anti-rabbit secondary antibodies (#K4003, Dako, Glostrup, Denmark) for 60 min at RT. This reaction was visualized using Alexa555-conjugated tyramide (#B40955, 1/200 dilution, Thermo Fisher, Waltham, MA, U.S.A.). For EdU revelation, after a washing step of 10 min in TBS/Tween 0.1%, slides were incubated for 30 min at RT with a TBS solution containing 4 mM $CuSO_4$, 8 mM sulfo-Cy3 azide, and 100 mM sodium ascorbate. After a washing step in PBS, nuclei were stained with Hoechst 33342 (Abcam, Cambridge, U.K.) and slides were mounted with Dako Fluorescent Mounting medium.

Fluorescence immunostained liver sections were digitalized using a Pannoramic 250 FlashIII scanner (3DHistech, Budapest, Hungary) at $\times$20 magnification. Scanned slides were then analyzed using the image analysis tool Author version 2017.2 (Visiopharm, Hørsholm, Denmark). On each slide, tissue sections were automatically surrounded at low magnification. Delineations were visually checked and manually corrected if required. Cells were then detected at high resolution ($\times$20) with a nucleus-based cell classification relying on Hoechst labeling. Following segmentation, post-processing steps were applied to separate Ki67+/− and EdU+/− cells. The parameters were constant for all slides. Results were expressed as permillage of stained cells. We assumed that hepatocellular nuclei appear as vague spheres and, on histological sections, as circles. Thus, $V = 4/3\ \pi\ r^3$, where V is the volume of the sphere, π is the Archimedes' constant, r is the radius, and $A = \pi\ r^2$, where A is the area of the circle. Therefore, $A = \pi\ (3/4\ V/\pi)^{2/3}$ where V is the mean volume of non-neoplastic hepatocytes (287 μm^3) reported by Jack et al. [39]. The average nuclear area of rat hepatocytes is consequently 50–53 μm^2 [39,40]. Nuclei larger than 40 μm^2 were considered to pertain to hepatocytes. This threshold was chosen to accommodate for the different levels at which nuclei might have been cut.

RNA extraction, cDNA synthesis, and real-time quantitative polymerase chain reaction

Total RNA was extracted from homogenized rat liver with the RNeasy Mini kit (Qiagen, Hilden, Germany) including on-column DNaseI treatment. RNA purity and quantity were measured by NanoDrop spectrophotometry, and 1 μg total RNA (A260/280 ratio of 2.03 $\pm$ 0.04) used to synthesize cDNA in the presence of 2 μl Random Primers using the High Capacity cDNA Reverse Transcription Kit (Thermo Fisher) as per manufacturer's instructions. cDNA

Downloaded from http://portlandpress.com/clinsci/article-pdf/135/19/2285/921840/cs-2021-0183.pdf by Universita degli Studi di Milano user on 18 October 2021

© 2021 The Author(s). Published by Portland Press Limited on behalf of the Biochemical Society

PORTLAND PRESS

samples were diluted 1:10 and 2 μl used in 25 μl real-time quantitative polymerase chain reaction (RT-qPCR) together with 12.5 μl SYBR Select Master Mix (Thermo Fisher), 1 μl of sequence-specific forward primer and 1 μl of sequence-specific reverse primer (Invitrogen, Carlsbad, CA, U.S.A.), and 8.5 μl sterile water. The primers are detailed below. Ribosomal Protein L19 (RPL19), i.e. the internal reference gene: forward CAAGCGGATTCTCATGGAACA, #128363, R4653 (A03), reverse TGGTCAGCCAGGAGCTTCTT, #128363, R4653 (A04); vascular endothelial growth factor-α (VEGFα): forward ATAGCAGATGTGAATGCAGACCA, #154160, R7216 (B09), reverse TCACAGTGAACGTCCAGGA, #154160, R7216 (B10); platelet-derived growth factor-β (PDGFβ): forward GGTGAGAAAGATCGAATTGT, #011376, R7603 (B07), reverse GAGTTTGAGGTGTCTTGGCT, #011376, R7603 (B08); angiopoietin-2 (AGPT2): forward GCTGGGCAACGAGTTTGTCT, #011376, R7603 (F01), reverse CAGTCCTTCAGCTGGATCTTCA, #011376, R7603 (F02). RT-qPCR assays were run in duplicates on a Rotor-Gene Q (Qiagen, Hilden, Germany) in 72-well plates over 45 cycles of 95°C for 15 s and 60°C for 60 s in a two-step thermal cycle preceded by an initiation step of 95°C for 10 min. RT-qPCR C_t values were acquired with the Rotor-Gene Q Series Software (Qiagen, Hilden, Germany) and relative gene expression calculated by the $2^{-\Delta C_t}$ method. The results were normalized for baseline expression in control rats.

RNA sequencing

Sequence libraries were prepared from the liver RNA extracts with the Lexogen QuantSeq 3′ mRNA-Seq library prep kit according to the manufacturer's protocol. Samples were indexed to allow for multiplexing. Library quality and size range was assessed using a Bioanalyzer (Agilent Technologies, Santa Clara, CA, U.S.A.) with the DNA 1000 kit (Agilent Technologies). Libraries were subsequently sequenced on an Illumina HiSeq4000 instrument. Single-end reads of 50-bp length were produced with a minimum of 1 M reads per sample. Quality control of raw reads was performed with FastQC 0.11.7 [41]. Adapters were filtered with ea-utils fastq-mcf v1.05 [42,43]. Splice-aware alignment was performed with HiSAT2 against the *Rattus norvegicus* reference genome (genome build = Rnor6.0). Reads mapping to multiple loci in the reference genome were discarded. Resulting BAM files were handled with Samtools v1.5 [44]. Quantification of reads per gene was performed with HT-seq Count v2.7.14. Count-based differential expression analysis was done with R-based Bioconductor package DESeq2 [45]. Reported *P*-values were adjusted for multiple testing with the Benjamini–Hochberg procedure, which controls false discovery rate (FDR). The raw RNA sequencing (RNAseq) data are available from http://www.ncbi.nlm.nih.gov/bioproject/705692.

Results from the DESeq2 package were used to perform Over-Representation Analysis (ORA) and Gene Set Enrichment Analysis (GSEA) with the WebGestaltR package [46]. These analyses were made on six reference sets including *Biological Process* (BP), *Cellular Component* (CC), and *Molecular Function* (MF), from *Gene Ontology* (GO) [47,48], the *Kyoto Encyclopedia of Genes and Genomes* (KEGG) [49], the *Reactome* [50], and from the *Panther* databases [51].

Statistical analysis

Continuous variables were reported as medians and interquartile ranges (IQRs). Differences in medians were tested with the Mann–Whitney U test. Overall differences in distributions between groups were tested with the Kruskal–Wallis omnibus test. Post-hoc tests were run to identify single differences by adjusting for multiple testing (Dunn's test). Dichotomous variables were explored using the maximum likelihood χ^2 test or the Fisher's exact test as appropriate. Significance was retained at $P<0.05$. Analyses were run with SPSS 25.0 (IBM Corp., Armonk, NY, U.S.A.) and GraphPad Prism 8.0 (GraphPad Software Inc., San Diego, CA, U.S.A.).

Results

Pharmacological pilot study

Roxadustat was well tolerated. HIF1α nucleus-cytoplasm ratio was higher, 1 h after injection, only in RXD25 compared with baseline. VEGF gene expression was higher in RXD25 than in RXD10 or in HAL, 1 h after injection. Likewise it was higher than in HAL 6 h after injection. At 6 h, PDGFβ gene expression was higher in RXD25 than in HAL, the expression of AGPT2 was higher in RXD25 than in RXD10 (Figure 2). As roxadustat stabilized liver HIF1α and drove an HIF-related gene signature only at 25 mg/kg, this dosage was chosen to proceed further.

Surgery

Operations took 40 (IQR = 38–45) min to be completed, with no differences between groups (Supplementary Information S1). The hepatectomy entailed a similar removal of 6.2 g of mass (IQR = 6.0–6.8, P=0.229). The remnant liver, estimated from a pool of rats of comparable age and body weight, amounted to 2.7 g (IQR = 2.6–2.9). The absolute

Downloaded from http://portlandpress.com/clinsci/article-pdf/135/19/2285/921840/cs-2021-0183.pdf by Universita degli Studi di Milano user on 18 October 2021

© 2021 The Author(s). Published by Portland Press Limited on behalf of the Biochemical Society

Clinical Science (2021) **135** 2285–2305
https://doi.org/10.1042/CS20210183

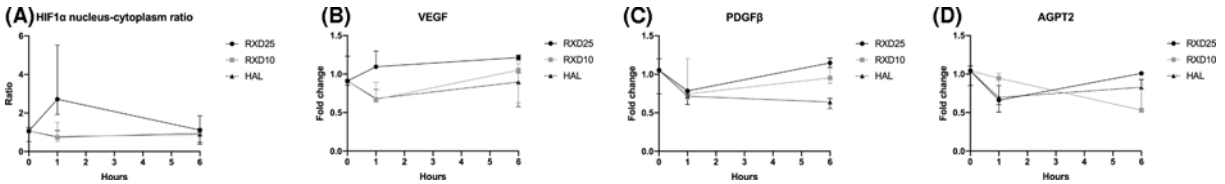


Figure 2. Preliminary evaluation of HIF-signaling pathway activation

(**A**) HIF1α nucleus-cytoplasm ratio, at 1 h, in RXD25 vs. baseline (P=0.042). (**B**) VEGF gene expression, at 1 h, in RXD25 vs. RXD10 (P=0.047), and vs. HAL (P=0.047). VEGF gene expression, at 6 h, in RXD25 vs. HAL (P=0.037). (**C**) PDGFβ gene expression, at 6 h, in RXD25 vs. HAL (P=0.044). (**D**) AGPT2 gene expression, at 6 h, in RXD25 vs. RXD10 (P=0.044). Given the exploratory nature of this phase, results are not corrected for multiple testing. Data shown as medians and IQR.

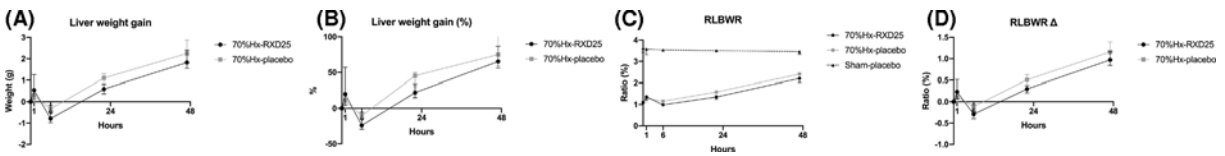


Figure 3. Evolution of remnant-liver-to-body-weight ratio and liver weight over time

(**A**) Resected rats exhibited a similar liver weight gain, at all time points but d1 (70%Hx-RXD25 vs. 70%Hx-placebo P=0.025). (**B**) Resected rats exhibited a similar percentage of liver weight gain, at all time points but d1 (70%Hx-RXD25 vs. 70%Hx-placebo P=0.025). (**C**) Resected rats exhibited a similar RLBWR, at all time points but d1 (70%Hx-RXD25 vs. 70%Hx-placebo P=0.016). (**D**) Resected rats exhibited a similar difference in RLBWR rise, at all time points but d1 (70%Hx-RXD25 vs. 70%Hx-placebo P=0.013). Data shown as medians and IQR. Abbreviation: RLBWR, remnant-liver-to-body-weight ratio.

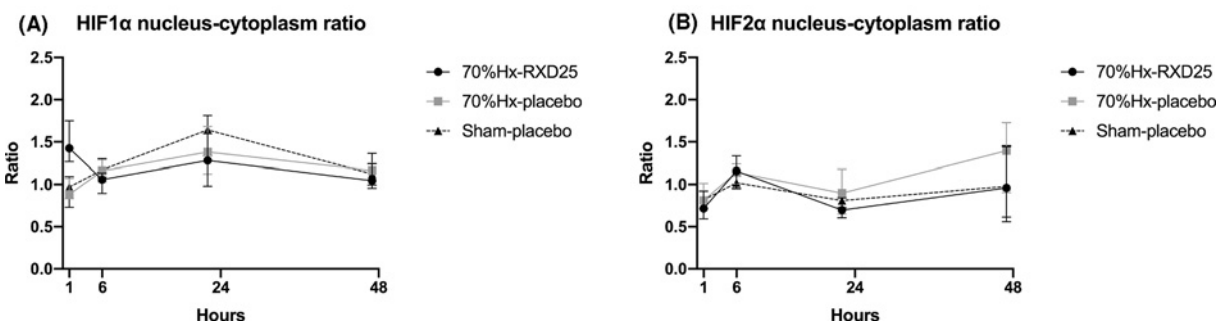


Figure 4. Post-operative evolution of HIF1α and HIF2α in the liver

(**A**) HIF1α nucleus-cytoplasm ratio in 70%Hx-RXD25 vs. 70%Hx-placebo (P=0.022) at 1 h after the end of surgery and drug administration. (**B**) HIF1α nucleus-cytoplasm ratio comparable among groups at all time points. Data shown as medians and IQR.

and relative growth of the liver remnant was comparable between the two operated groups at all time points except for d1, when 70%Hx-RXD25 rats showed a reduced liver weight gain compared with 70%Hx-placebo (Figure 3).

HIF1α and HIF2α stabilization

The HIF1α nucleus-cytoplasm ratio was greater in 70%Hx-RXD25 livers compared with 70%Hx-placebo at 1 h (P=0.022). After this first time point, no differences between groups were detected. At no time point, the HIF2α nucleus-cytoplasm ratio was significantly different among the three groups (Figure 4).

Complete blood count

The red blood cell count showed that, only in 70%Hx-RXD25, there was a surge in red blood cell count on d2 compared with d1 (P<0.001), and with 6 h (P=0.003). Concordantly, hemoglobin concentration was greater on d2 compared with d1 (P<0.001), and almost significantly greater if compared with 6 h (P=0.050), hematocrit was greater on d2 compared with d1 (P<0.001), and to 6 h (P=0.003) Platelet count was greater in 70%Hx-RXD25 compared with 70%Hx-placebo and sham-placebo on d1. Peripheral white blood cells count was higher in 70%Hx-RXD25 compared

© 2021 The Author(s). Published by Portland Press Limited on behalf of the Biochemical Society

Downloaded from http://portlandpress.com/clinsci/article-pdf/135/19/2285/921840/cs-2021-0183.pdf by Universita degli Studi di Milano user on 18 October 2021

with 70%Hx-placebo on d2. This divergence is accounted for by differences in lymphocytes and monocytes (Figure 5).

Plasma analytes

Resected rats exhibited a similar rise in transaminases compared with sham-placebo, with a peak on d1 and a partial decline on d2 (Figure 6). While albumin levels are overall stable after liver resection, resected rats showed lower levels on d1 compared with sham-placebo. We observed an increase in factor V concentration in resected rats on d1, with no difference between 70%Hx-RXD25 and 70%Hx-placebo. Ammonia levels were higher in 70%Hx-RXD25 than in sham-placebo at 1, 22, and 47 h after hepatectomy. On d1 and d2, lactate levels were higher in 70%Hx-RXD25 than in sham-placebo. Similarly, total bilirubin in 70%Hx-RXD25 showed a modest but significant increase compared with sham-placebo on d1 and d2, and with 70%Hx-placebo only on d1. On d1, pH was higher in 70%Hx-RXD25 than in sham-placebo. Creatinine was within normal range at all time points.

Gd-EOB-DTPA MRI

On d1, the time to peak was similar among groups. AUC60 was significantly reduced in 70%Hx-RXD25 compared with 70%Hx-placebo and with sham-placebo. AUC90 data followed a similar trend (not shown). Accordingly, the AUC from t0 to peak, which accounts for contrast uptake, was reduced in 70%Hx-RXD25 compared with sham-placebo. The total AUC, which accounts for total contrast exposure, was one-third in 70%Hx-RXD25 compared with 70%Hx-placebo and sham-placebo, though the time for 30% decrease was similar among groups. On d2, except for the time to peak that was longer in 70%Hx-RXD25 than in 70%Hx-placebo, no parameter showed significant differences (Figure 7).

Survival

We recorded comparable survival rates, with only 4 events out of 34 animals in the 70%Hx-RXD25. All the events happened during or soon after d1 MRI (Supplementary Information S2).

Immunofluorescence

While unaffected on d1, the proportion of Ki67-stained cells, increased significantly on d2 in regenerating lobes, with no differences between 70%Hx-RXD25 and 70%Hx-placebo. Hepatocytes, i.e., liver cells with large round nucleus, were the main contributor to this increase. A similar behavior was observed at EdU immunofluorescence, labeling cells in S-phase of cell cycle (Figures 8 and 9).

Histology

Mitoses were not detected on d1 and were extensively displayed on d2 in resected rats without differences between 70%Hx-RXD25 and 70%Hx-placebo. On d1, inflammation, endothelial denudation, microvascular thrombosis, parenchymal hemorrhage, and necrosis were virtually absent from all sections. Hepatocellular ballooning was detected in all 70%Hx-placebo samples but only in 2/13 70%Hx-RXD25 and in 1/8 sham-placebo. Steatosis occurred in all but one 70%Hx-placebo samples, mainly as microvesicular and midzonal. In contrast, fatty infiltration was detected in only 5/13 of liver remnants in the 70%Hx-RXD25 group. When steatosis was present, its degree was less severe in 70%Hx-RXD25 than in 70%Hx-placebo (Figure 10).

On d2, inflammation, endothelial denudation, parenchymal hemorrhage, and necrosis were virtually absent from all sections. Only one instance of microvascular thrombosis was detected in the 70%Hx-placebo group. Hepatocellular ballooning was milder and clearly detectable only in one case of 70%Hx-RXD25. Steatosis lost zonation and was generally diffuse, appearing in all cases of resected rats without differences in proportion or in degree (Table 1).

RNAseq

The relief from hepatocellular ballooning and steatosis, the only significant effect of roxadustat as opposed to placebo in the context of 70%Hx, was identified after 22 h from roxadustat administration. Liver samples coming from the three experimental groups underwent analysis of global transcriptome changes with an RNAseq approach. The analysis is reported in Supplementary Information S3. We detected 2521 genes whose expression was significantly different in 70%Hx-RXD25 compared with 70%Hx-placebo. The principal component analysis separated the samples according to the treatment. We employed ORA to determine if the significantly modulated genes likely originated from any known gene pathways, while GSEA was performed to assess the enrichment of up- or down-regulated genes in these pathways. We identified nine clusters of cellular functions that were recurrently enriched in 70%Hx-RXD25 compared

Downloaded from http://portlandpress.com/clinsci/article-pdf/135/19/2285/921840/cs-2021-0183.pdf by Universita degli Studi di Milano user on 18 October 2021

© 2021 The Author(s). Published by Portland Press Limited on behalf of the Biochemical Society

Clinical Science (2021) **135** 2285–2305
https://doi.org/10.1042/CS20210183

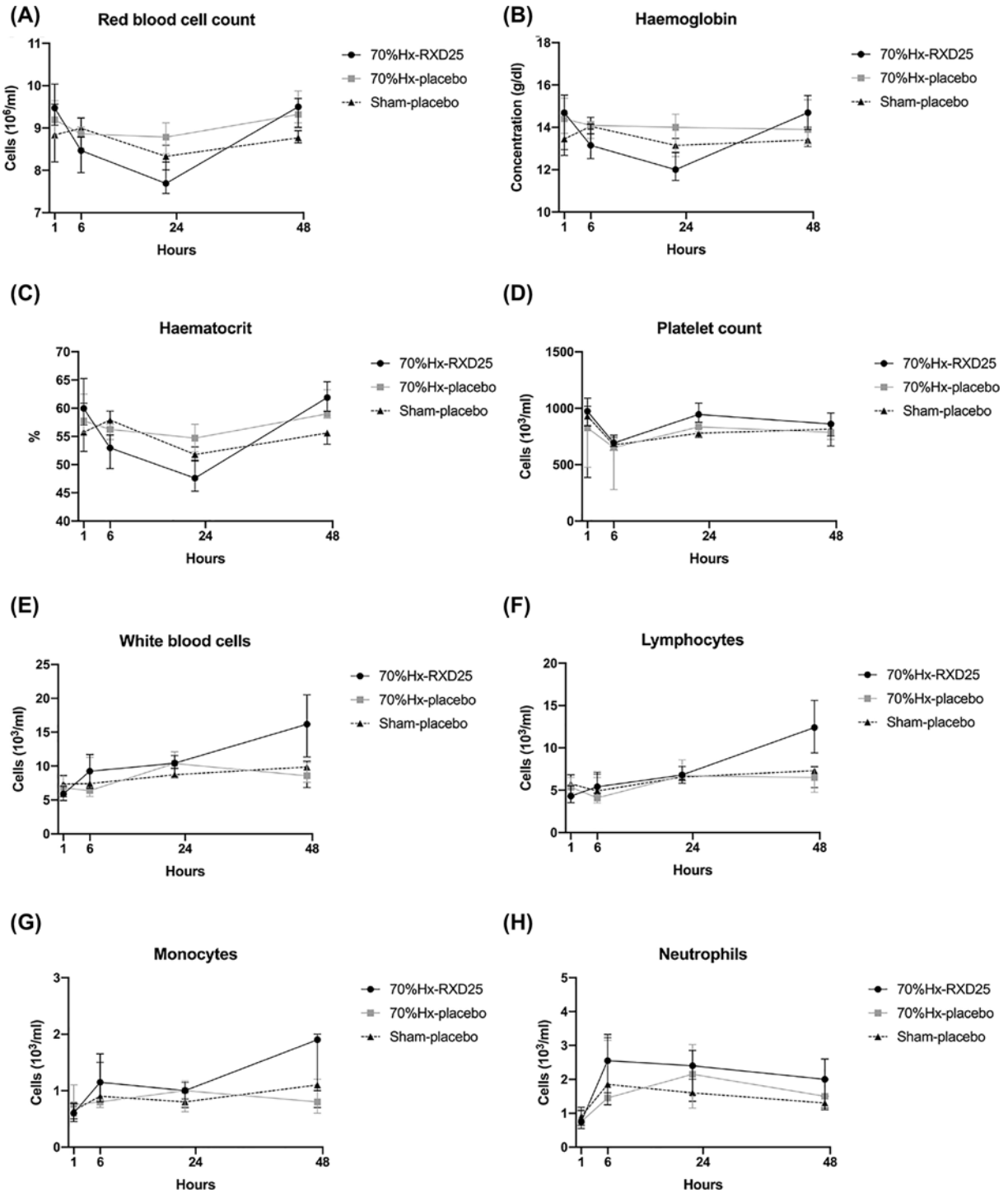


Figure 5. Complete blood count

(**A**) Erythrocytes. On d1, 70%Hx-RXD25 vs. 70%Hx-placebo (P=0.012). On d2, 70%Hx-RXD25 vs. sham-placebo (P=0.012). (**B**) Hemoglobin. On d1, 70%Hx-RXD25 vs. 70%Hx-placebo (P=0.005). On d2, 70%Hx-RXD25 vs. sham-placebo (P=0.030). (**C**) Hematocrit. At 6 h, 70%Hx-RXD25 vs. sham-placebo (P=0.019). On d1, 70%Hx-RXD25 vs. 70%Hx-placebo (P=0.013). On d2, 70%Hx-RXD25 vs. sham-placebo (P<0.001). (**D**) Platelets. On d1, 70%Hx-RXD25 vs. 70%Hx-placebo (P=0.007), and vs. sham–placebo (P<0.001). (**E**) Leukocytes. On d2, 70%Hx-RXD25 vs. 70%Hx-placebo (P=0.012). (**F**) Lymphocytes. On d2, 70%Hx-RXD25 vs. 70%Hx-placebo (P=0.004) and vs. sham-placebo (P=0.031). (**G**) Monocytes. On d2, 70%Hx-RXD25 vs. 70%Hx-placebo (P=0.031). (**H**) Neutrophils. No statistically significant differences. Data shown as medians and IQR.

Downloaded from http://portlandpress.com/clinsci/article-pdf/135/19/2285/921840/cs-2021-0183.pdf by Universita degli Studi di Milano user on 18 October 2021

© 2021 The Author(s). Published by Portland Press Limited on behalf of the Biochemical Society

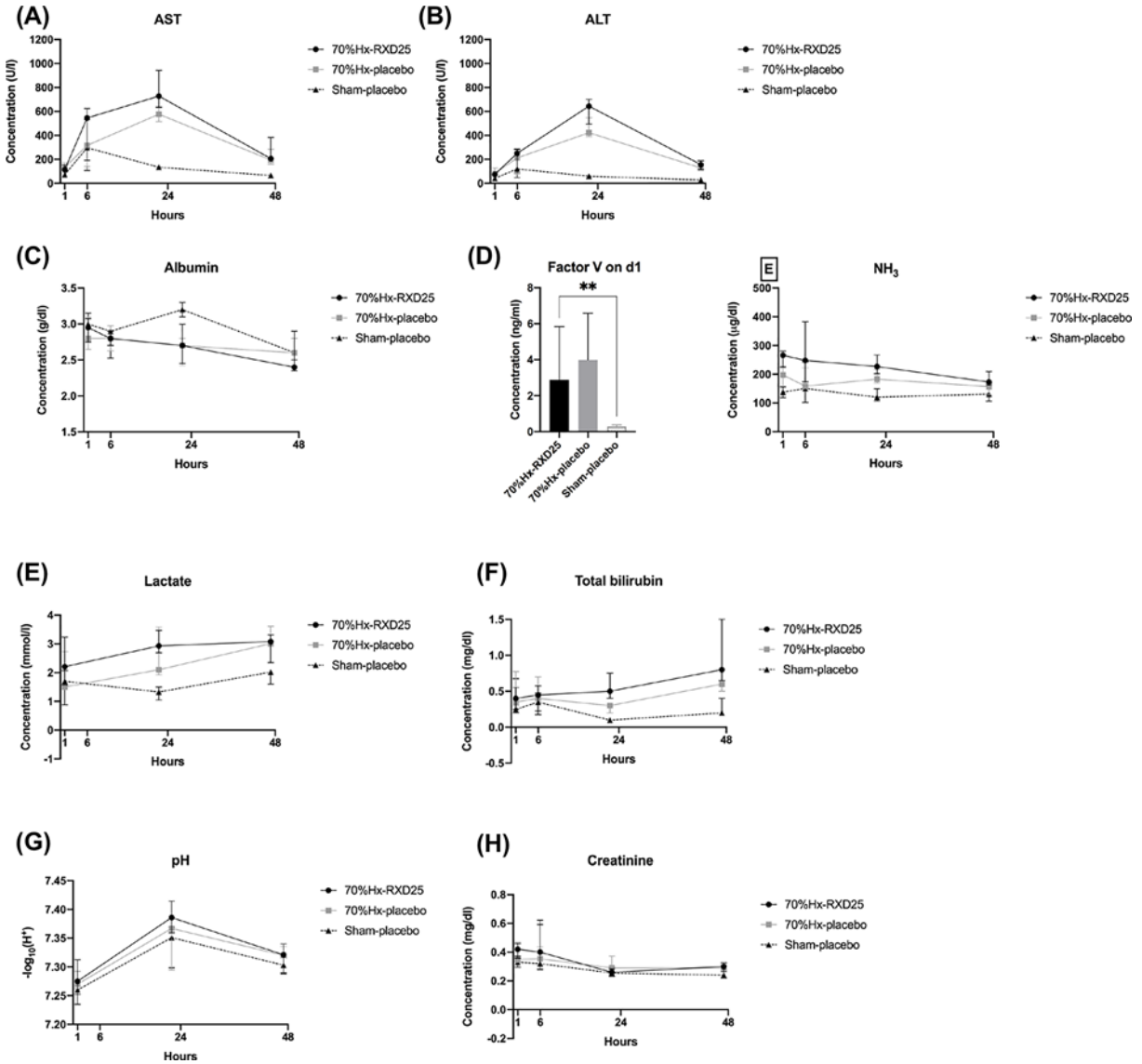


Figure 6. Evolution of plasma analytes over time

(**A**) AST on d1, 70%Hx-RXD25 vs. 70%Hx-placebo (P=0.279), and vs. sham-placebo (P<0.001); on d2, 70%Hx-RXD25 vs. 70%Hx–placebo (P=0.923), and vs. sham-placebo (P<0.001). (**B**) ALT on d1, 70%Hx-RXD25 vs. 70%Hx-placebo (P=0.308), and vs. sham–placebo (P<0.001); on d2, 70%Hx-RXD25 vs. 70%Hx-placebo (P=0.922), and vs. sham-placebo (P<0.001). (**C**) Albumin on d1, 70%Hx-RXD25 vs. 70%Hx-placebo (P=1.000), and vs. sham-placebo (P=0.002). (**D**) Factor V on d1, 70%Hx-RXD25 vs. 70%Hx–placebo (P=1.000), and vs. sham-placebo (P=0.003). (**E**) Ammonia in 70%Hx-RXD25 vs. sham-placebo after 1 (P=0.009), 22 (P<0.001), and 47 h (P=0.012) after surgery. (**F**) Lactate in 70%Hx-RXD25 vs. sham-placebo on d1 (P<0.001) and on d2 (P=0.006). (**G**) Total bilirubin in 70%Hx-RXD25 vs. 70%Hx-placebo on d1 (P=0.025) and vs. sham-placebo on d1 (P<0.001) and on d2 (P=0.002). (**H**) pH in 70%Hx-RXD25 vs. sham-placebo on d1 (P=0.035). (**I**) Creatinine within normal range. Data shown as medians and IQR.

with 70%Hx-placebo. Three of those pathway clusters appeared generally up-regulated: HIF signaling, energy production via oxidative phosphorylation, and lipid metabolism, while six pathway clusters were down-regulated: cell growth and death, oxidative stress, xenobiotic metabolism, transmembrane transporters, inflammation, endocrine signaling (Supplementary Information S4). The comparison between the 70%Hx-RXD25 group and the sham-placebo group showed that the former exhibits an up-regulation of cell cycle genes and the HIF1α pathway. The comparison between the 70%Hx-placebo group and the sham-placebo group showed that the former exhibits an up-regulation of

Downloaded from http://portlandpress.com/clinsci/article-pdf/135/19/2285/921840/cs-2021-0183.pdf by Universita degli Studi di Milano user on 18 October 2021

© 2021 The Author(s). Published by Portland Press Limited on behalf of the Biochemical Society

Clinical Science (2021) **135** 2285–2305
https://doi.org/10.1042/CS20210183

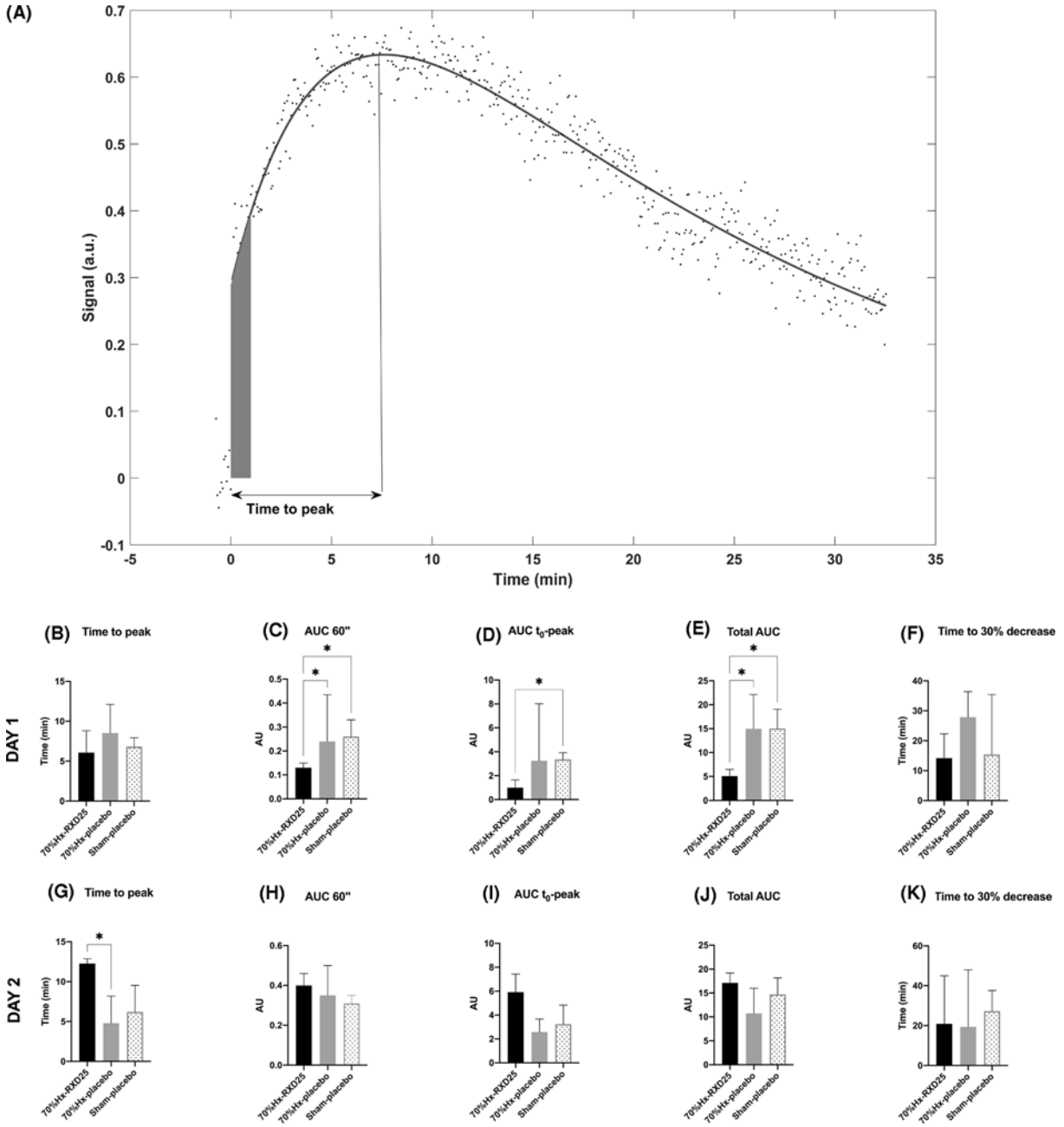


Figure 7. Results of the Gd-EOB-DTPA MRI

(**A**) Example of MRI normalized signal analysis. The area in gray marks the AUC60″. (**B**) d1 time to peak similar among groups (Kruskal–Wallis P=0.594). (**C**) d1 AUC60 in 70%Hx-RXD25 vs. 70%Hx-placebo (P=0.013), and vs. sham-placebo (P=0.035). (**D**) d1 AUC from t_0 to peak in 70%Hx-RXD25 compared with sham-placebo (P=0.035). (**E**) d1 total AUC in 70%Hx-RXD25 vs. 70%Hx–placebo (P=0.012) and vs. sham (P=0.012). (**F**) d1 time to 30% signal decrease (Kruskal–Wallis P=0.300). (**G**) d2 time to peak in 70%Hx-RXD25 vs. 70%Hx-placebo (P=0.027). (**H**) d2 AUC60 (P=0.813). (**I**) d2 AUC from t_0 to peak (Kruskal–Wallis P=0.085). J: d2 total AUC (Kruskal–Wallis P=0.291). (**K**) d2 time to 30% signal decrease (Kruskal–Wallis P=0.910). *$P<0.050$. Data shown as medians and IQR.

Downloaded from http://portlandpress.com/clinsci/article-pdf/135/19/2285/921840/cs-2021-0183.pdf by Universita degli Studi di Milano user on 18 October 2021

© 2021 The Author(s). Published by Portland Press Limited on behalf of the Biochemical Society

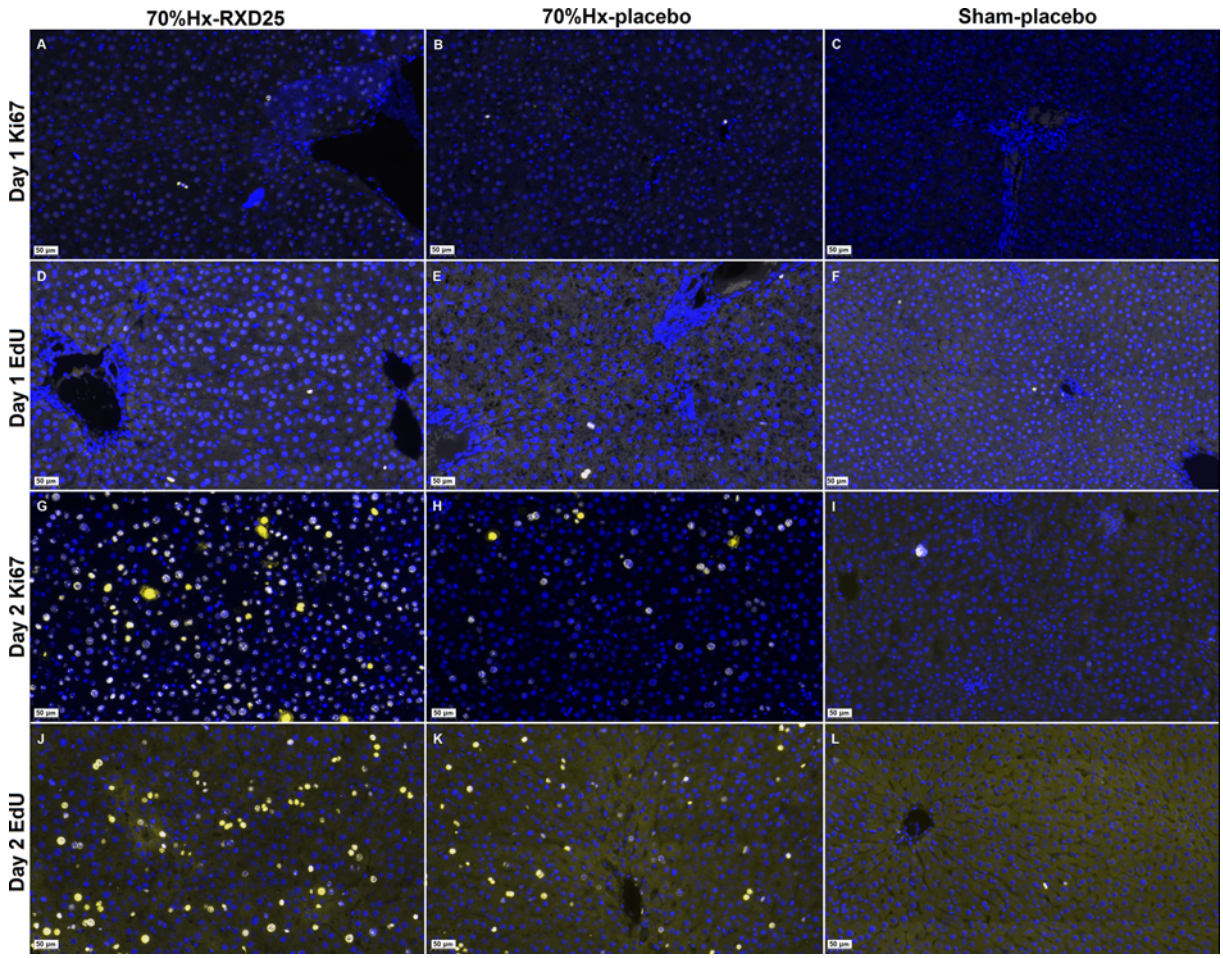


Figure 8. Immunofluorescence for Ki67 and EdU (×20)

Positive nuclei are labeled in yellow, filter SP Gold, 555 nm. (**A**) d1 70%Hx-RXD25 Ki67-positive cells. (**B**) d1 70%Hx-placebo Ki67-positive cells. (**C**) d1 sham-placebo Ki67-positive cells. (**D**) d1 70%Hx-RXD25 EdU-positive cells. (**E**) d1 70%Hx-placebo EdU-positive cells. (**F**) d1 sham-placebo EdU-positive cells. (**G**) d2 70%Hx-RXD25 Ki67-positive cells. (**H**) d2 70%Hx-placebo Ki67-positive cells. (**I**) d2 sham-placebo Ki67-positive cells. J: d2 70%Hx-RXD25 EdU-positive cells. (**K**) d2 70%Hx-placebo EdU–positive cells. (**L**) d2 sham-placebo EdU-positive cells.

cell cycle genes. Both resected groups showed a down-regulation in lipid metabolism genes as opposed to the sham group (Supplementary Information S5 and Figures 11-12).

Discussion

Liver resection causes a rapid induction of HIF1α-associated main intracellular signaling pathways in a murine model of both standard (68%) and extended liver resection (86%) [52]. Activation of HIF-driven pathways could be a consequence of the immediate post-resection hypoxic conditions, caused by the overflow of oxygen-poor portal blood in a partially resected liver and the consequent buffering reduction in oxygen-rich arterial supply. This ischemic phase is probably required to trigger the early phase of liver regeneration [5]. Interestingly, no later than 32 h after standard two-third hepatectomy, hypoxia-induced pathways are rapidly down-regulated. Hypoxia may thus be an important fine-tuning mechanism to induce liver regeneration [52], which acts in the very first days after liver resection. This might explain why even extreme resections performed in the setting of a reinforced hypoxia evolve favorably [4].

This is the first reported experience with roxadustat, a selective HIF stabilizer, in partial liver resection. In terms of safety, roxadustat tolerance was unexplored in this kind of hepatobiliary surgery. Data in the literature report that healthy adult rats should well tolerate a single dose of Roxadustat 25 mg/kg [25]. A few roxadustat-treated rats, but

Downloaded from http://portlandpress.com/clinsci/article-pdf/135/19/2285/921840/cs-2021-0183.pdf by Universita degli Studi di Milano user on 18 October 2021

© 2021 The Author(s). Published by Portland Press Limited on behalf of the Biochemical Society

Clinical Science (2021) **135** 2285–2305
https://doi.org/10.1042/CS20210183

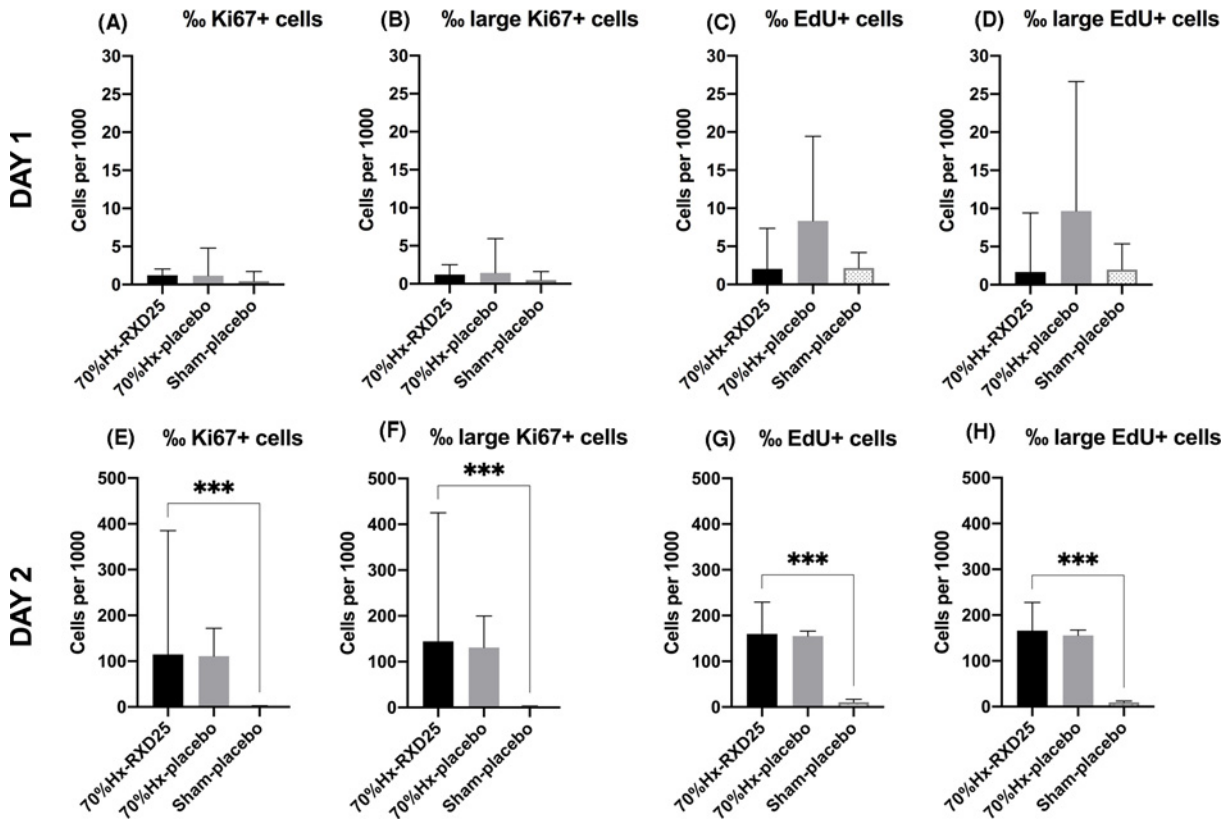


Figure 9. Results of immunofluorescence for Ki67 and EdU

(**A**) d1 Ki67-positive cells (Kruskal–Wallis P=0.391). (**B**) d1 large Ki67-positive cells (Kruskal–Wallis P=0.483). (**C**) d1 EdU-positive cells (Kruskal–Wallis P=0.129). (**D**) d1 large EdU-positive cells (Kruskal–Wallis P=0.107. (**E**) d2 Ki67-positive cells in 70%Hx-RXD25 vs. sham-placebo (Dunn's $P<0.001$). (**F**) d2 large Ki67-positive in 70%Hx-RXD25 vs. sham-placebo (Dunn's $P<0.001$). (**G**) d2 EdU-positive cells in 70%Hx-RXD25 vs. sham-placebo (Dunn's $P<0.001$). (**H**) d2 large EdU-positive cells in 70%Hx-RXD25 vs. sham-placebo (Dunn's $P<0.001$). ***$P<0.001$. Data shown as medians and IQR.

none of the placebo-treated, died on the first day after liver resection. Remarkably, death occurred during of immediately after MRI imaging, suggesting that roxadustat might result from a reduced tolerance to prolonged anesthesia after liver resection. Besides, we cannot fully exclude an unexpected toxicity from the association between roxadustat and Gd-EOB-DTPA.

While liver HIF1α stabilization vanishes by the sixth hour from roxadustat administration, RNAseq confirmed that the roxadustat-induced up-regulation of HIF1α-associated pathways is detectable at least until 22 h later. Similarly, the rise in the erythroid lineage on d2 along with the increased platelet release on d1 [53] support the evidence for an efficient HIF1α stabilization. Roxadustat has been indeed developed to raise the levels of erythropoietin and, upon roxadustat administration, we registered a blood cell response. Moreover, erythropoietin *per se* exerts an influence on liver regeneration and metabolism, by inducing hepatic proliferation and decreasing lipid accumulation in the liver [54,55]. Then we additionally measured the plasma levels of erythropoietin to investigate whether our findings could be partly explained by a raise in erythropoietin release but the results did not confirm this hypothesis (Supplementary Information S6).

At variance with data concerning genetic PHD1 silencing in a murine model of liver ischamia [56], we could not detect a roxadustat-induced differential HIF2α stabilization. Other less-selective PHD inhibitors prompted a response similar to ours: nucleus pulposus cells, once exposed to DMOG, showed an accumulation of HIF1α and an up-regulation of its target genes, but not of HIF2α [57]. These data, the evidence that both HIF1α and HIF2α are stabilized after hepatectomy [4], along with our experience suggest that proteasomal degradation of HIF2α is only partly or not primarily mediated by classical oxygen-dependent PHD pathway after liver resection.

© 2021 The Author(s). Published by Portland Press Limited on behalf of the Biochemical Society

Downloaded from http://portlandpress.com/clinsci/article-pdf/135/19/2285/921840/cs-2021-0183.pdf by Universita degli Studi di Milano user on 18 October 2021

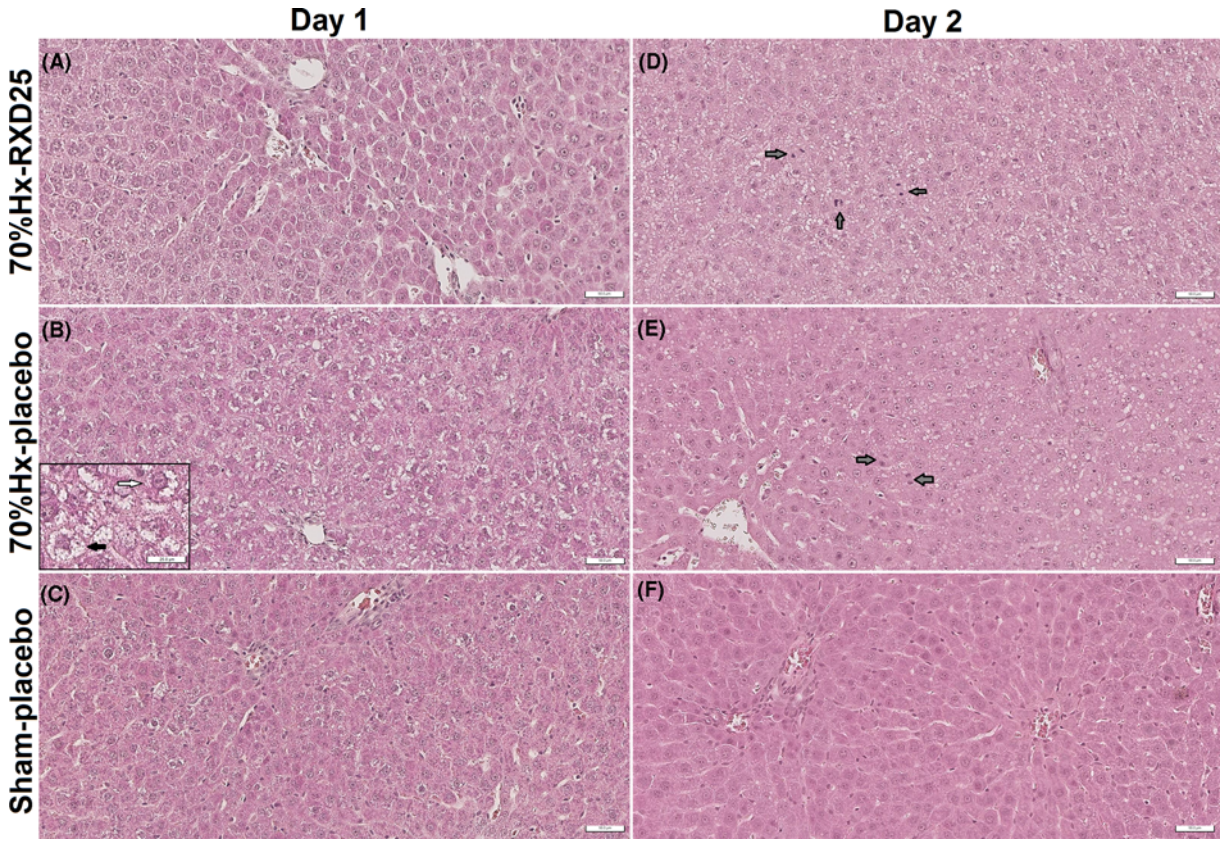


Figure 10. H&E-stained whole-liver sections (×20)

(**A**) d1 70%Hx-RXD25 slide showing minor steatosis and no ballooning. (**B**) d1 70%Hx-placebo slide. To the bottom right, a X40 magnified section showing an example of hepatocellular ballooning (black-filled arrow) and microvesicular steatosis (white-filled arrow). (**C**) d1 sham-placebo slide appearing essentially normal. (**D**) d2 70%Hx-RXD25 slide showing mild diffuse microvesicular steatosis and a number of mitotic figures (some examples are pointed out by grey-filled arrows). (**E**) d2 70%Hx-placebo slide showing mild diffuse microvesicular steatosis. (**F**) d2 sham-placebo slide appearing essentially normal.

Overall, hypoxia is supposed to coordinate murine liver regeneration by coupling parenchymal growth to vascular expansion [4,5]. However, because fatalities occur during the first 48 h after liver resection in murine models and hypoxia-driven response rapidly fades out after 32 h, the putative protective effect of HIF stabilization should entail very early functional adjustments consequent to changes in hepatocellular energetic status [58]. Therefore, beside morphological regeneration, we evaluated function, essential to claim that a treatment has an effect whatever on postoperative liver failure [59]. More than crude mortality rate, liver function is a reproducible and meaningful endpoint because it reflects the pathophysiology of human hepatocellular dysfunction in terms of synthesis, detoxification, inflammation, necrosis, and collateral damage [60].

Gd-EOB-DTPA uptake appeared generally hindered in roxadustat-treated resected rats as assessed by the reduction in AUC60 and AUC90 on d1, and the delay of the time to peak on d2 compared with 70%Hx-placebo and sham-placebo. Gd-EOB-DTPA employs organic anion-transporting polypeptides (OATPs) to enter hepatocytes following the electrochemical gradient across plasma membrane [61–63]. Thus, decreased AUC could correspond to a decreased uptake. Correspondingly, RNAseq confirmed that roxadustat specifically inhibited the expression of Slco1a1, the gene encoding OATP1, in the context of liver resection (Supplementary Information S3). Inversely, we did not detect a significant effect on Gd-EOB-DTPA biliary excretion, which relies on the ATP-dependent canalicular membrane multidrug resistance proteins [61–63]. We did not gather evidence that roxadustat improved hepatocellular function postoperatively. Yet, to our knowledge, this is the first established rat model of standard hepatectomy, in which hepatocellular function was detailed through contrast-enhanced MRI and which showed a substantial invariability in MRI parameters between sham-operated and 70%-liver resected rats. Previously, in a rat model of 70 and 90% liver resection, the vascular clearance of Gd-EOB-DTPA was utilized to identify liver function differences

Downloaded from http://portlandpress.com/clinsci/article-pdf/135/19/2285/921840/cs-2021-0183.pdf by Universita degli Studi di Milano user on 18 October 2021

© 2021 The Author(s). Published by Portland Press Limited on behalf of the Biochemical Society

Clinical Science (2021) **135** 2285–2305
https://doi.org/10.1042/CS20210183

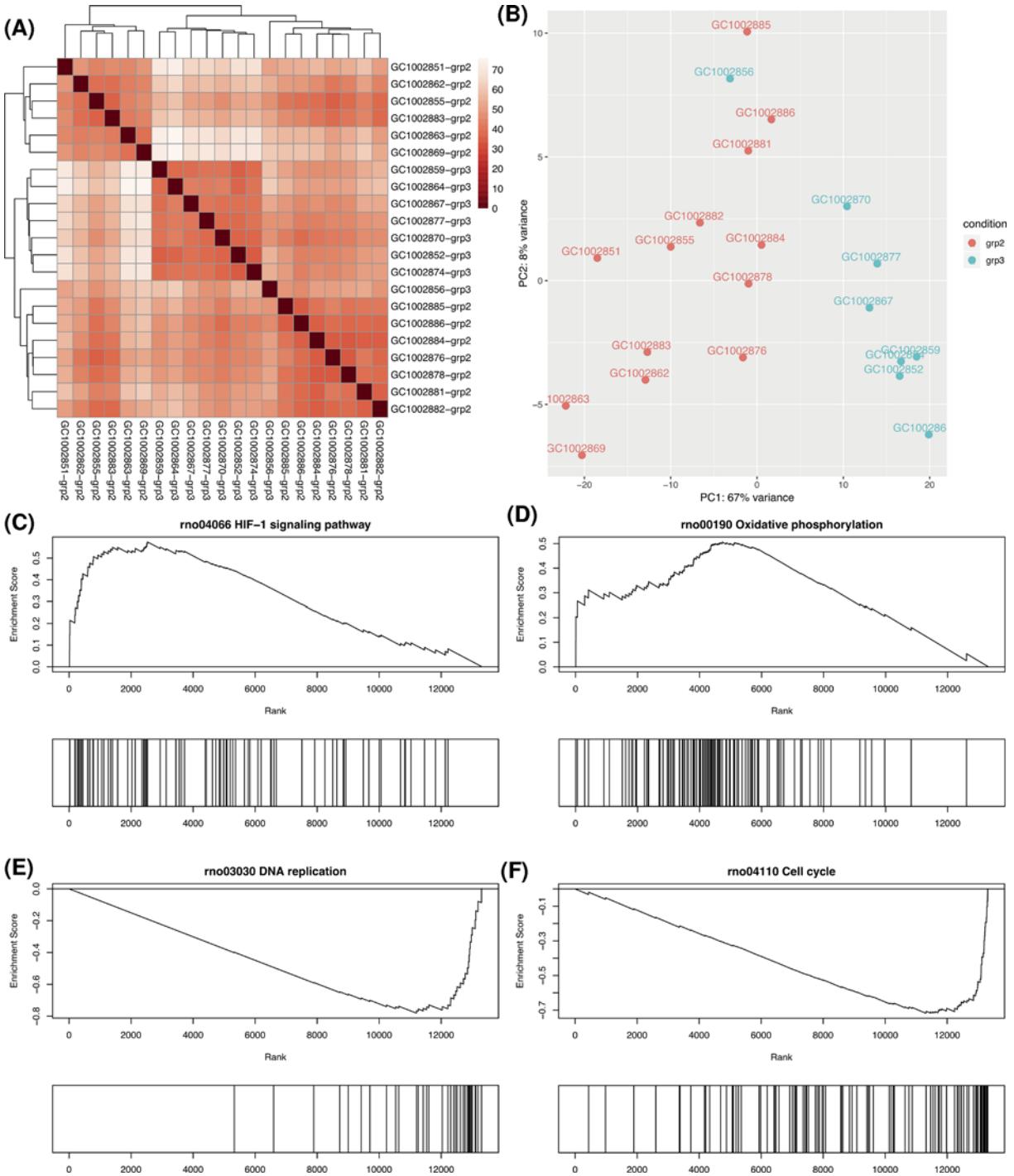


Figure 11. RNAseq

(**A**) Heatmap of the sample-to-sample distances. Sample clustering. (**B**) Principal component analysis. The plot shows the samples spanned in the 2D plane and grouped by their first two principal components, in order to visualize biases and batch effects. Grp2 = 70%Hx-RXD25, grp3 = 70%Hx-placebo. (**C–F**) Preranked enriched plots [81]. Excerpts from GSEA based on the KEGG database. (C) HIF1α-signaling pathway up-regulated in 70%Hx-RXD25 compared with 70%Hx-placebo. (D) Oxidative phosphorylation gene set up-regulated in 70%Hx-RXD25 compared with 70%Hx-placebo. (E) DNA replication gene set down-regulated in 70%Hx-RXD25 compared with 70%Hx-placebo. (F) Cell cycle gene set down-regulated in 70%Hx-RXD25 compared with 70%Hx-placebo.

Downloaded from http://portlandpress.com/clinsci/article-pdf/135/19/2285/921840/cs-2021-0183.pdf by Universita degli Studi di Milano user on 18 October 2021

© 2021 The Author(s). Published by Portland Press Limited on behalf of the Biochemical Society

Table 1 Histology report

	70%Hx-RXD25 (N (%))	70%Hx-placebo (N (%))	Sham-placebo (N (%))	*P*
Day 1				
Mitoses	0/13 (0.00)	0/8 (0.00)	0/8 (0.00)	-
Inflammation	0/13 (0.00)	0/8 (0.00)	0/8 (0.00)	-
Endothelial denudation	0/13 (0.00)	0/8 (0.00)	0/8 (0.00)	-
Microvascular thrombosis	0/13 (0.00)	0/8 (0.00)	0/8 (0.00)	-
Parenchymal hemorrhage	0/13 (0.00)	0/8 (0.00)	0/8 (0.00)	-
Necrosis	0/11 (0.00)	0/8 (0.00)	0/7 (0.00)	-
Hepatocellular ballooning	2/13 (15.38)	7/8 (87.50)[1]	1/8 (12.50)	0.001[2]
Steatosis (≥5%)	5/13 (38.46)	7/8 (87.50)[3]	1/8 (12.50)	0.005[2]
Degree of steatosis				
Undetectable (steatosis 0%)	3/13 (23.08)	1/8 (12.50)		0.028[4]
Healthy hepatocytes (steatosis < 5%)	5/13 (38.46)	0/8 (0.00)		
Mild (steatosis 5–33%)	5/13 (38.46)	4/8 (50.00)		
Moderate (steatosis 33–66%)	0/13 (0.00)	3/8 (37.50)		
Severe (steatosis > 66%)	0/13 (0.00)	0/8 (0.00)		
Day 2				
Mitoses	9/9 (100.00)	9/9 (100.00)[5]	1/7 (14.29)	<0.001[2]
Inflammation	0/9 (0.00)	0/9 (0.00)	0/7 (0.00)	-
Endothelial denudation	0/9 (0.00)	0/9 (0.00)	0/7 (0.00)	-
Microvascular thrombosis	0/9 (0.00)	1/9 (11.11)	0/7 (0.00)	0.347[2]
Parenchymal hemorrhage	0/9 (0.00)	0/9 (0.00)	0/7 (0.00)	-
Necrosis	0/9 (0.00)	0/8 (0.00)	0/7 (0.00)	-
Hepatocellular ballooning	1/7 (14.29)	0/9 (0.00)	0/7 (0.00)	0.289[2]
Steatosis (≥5%)	9/9 (100.00)	9/9 (100.00)[6]	1/7 (14.29)	<0.001[2]
Degree of steatosis				
Undetectable (steatosis 0%)	0/9 (0.00)	0/9 (0.00)		0.229[4]
Healthy hepatocytes (steatosis < 5%)	0/9 (0.00)	0/9 (0.00)		
Mild (steatosis 5–33%)	0/9 (0.00)	1/9 (11.11)		
Moderate (steatosis 33–66%)	9/9 (100.00)	8/9 (88.88)		
Severe (steatosis > 66%)	0/9 (0.00)	0/9 (0.00)		

[1]70%Hx-RXD25 vs. 70%Hx-placebo: Fisher's *P*=0.002.
[2]Maximum likelihood chi square test.
[3]70%Hx-RXD25 vs. 70%Hx-placebo: Fisher's *P*=0.067.
[4]Mantel–Haenszel test of trend.
[5]70%Hx-RXD25 vs. 70%Hx-placebo: Fisher's *P*=1.000.
[6]70%Hx-RXD25 vs. 70%Hx-placebo: Fisher's *P*=1.000.

in a plasma pharmacokinetic study [64]. In our experience, other measures of liver function did not appear to be influenced by roxadustat compared with 70%Hx-placebo. In particular, synthesis of albumin or factor V, clearance of lactate, ammonia or bilirubin, and transaminases showed no differences.

The current literature concerning the models of liver regeneration after hepatectomy almost invariably emphasizes results in terms of death rate, immunohistological measures of cell proliferation, and increase in remnant size [56], as proxies for improved liver regeneration or reduced SFSS [4,56]. However, while death is an inhumane endpoint [65], evidence coming from SFSS-associated rodent mortality can hardly be translated to humans [66]. Moreover, graft size is influenced by inflammation and edema, and it does not necessarily correlate with function. Finally, the fine-tuned study of liver function, much advocated in order to produce meaningful insights into the physiology of liver regeneration, should be routinely reported [67].

After extreme resections, liver regains mass for up to 7 days and the difference between livers exposed to hypoxia or not peaks on postoperative day 3 [4]. In the standard model of liver resection we used, there is little room for improvement because the hepatostat is reached within 3 days after 70%Hx [68]. Liver growth, as we assessed by size measurement, proved actually similar between the treatment groups, in keeping with the evidence coming from ki67 staining, EdU labeling, and mitoses count. Our results are not in line with previous research with PHD inhibitors.

Downloaded from http://portlandpress.com/clinsci/article-pdf/135/19/2285/921840/cs-2021-0183.pdf by Universita degli Studi di Milano user on 18 October 2021

© 2021 The Author(s). Published by Portland Press Limited on behalf of the Biochemical Society

Clinical Science (2021) **135** 2285–2305
https://doi.org/10.1042/CS20210183

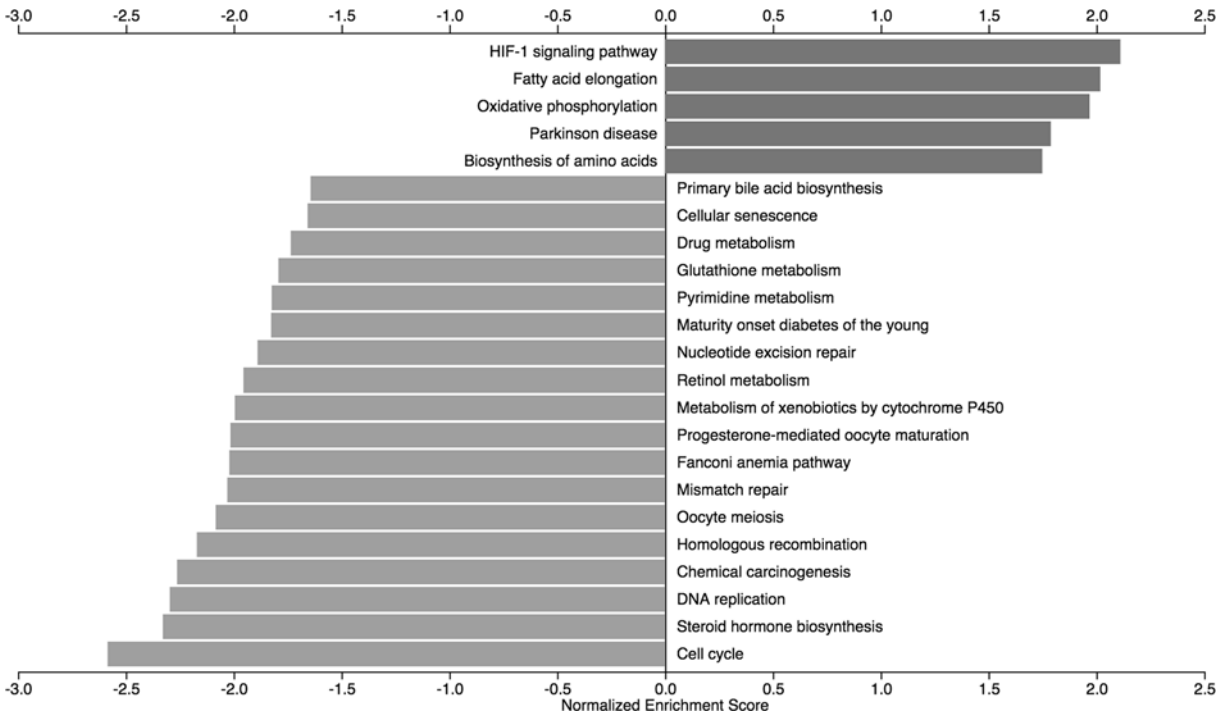


Figure 12. GSEA based on the KEGG database, showing only gene sets with FDR $P<0.05$

Harnoss et al. observed that EDHB improved hepatocellular proliferation, measured on d2 after 75% hepatectomy [9]. Correspondingly, EDHB induced cyclin D1 and cyclin D2 up-regulation after liver resection. These effects are HIF2α-dependent [69], and, while the authors did not show the differential profile of HIF1α–HIF2α stabilization in their experience, it is safe to assume that the growth-promoting effects of EDHB are mediated by an increase transactivity of HIF2α via a non-selective inhibition of its degradation. Whether this HIF2α stabilization is obtained via the inhibition of PHDs or other dioxygenases or a mix of the two remains unclear, because in our experience roxadustat, which effectively and selectively inhibits PHDs, stabilized only HIF1α and did not promote liver regeneration after hepatectomy. Conversely, the data coming from RNAseq unanimously underline that the HIF1α-stabilizing treatment dampens cell cycle progression.

The most relevant effect observed upon the administration of roxadustat in 70%Hx was a marked improvement in hepatocellular ballooning and steatosis, known hallmarks of hepatocellular stress, on d1. Fatty infiltration of the liver after partial resection has been known for 70 years [70]. After hepatectomy, circulating fatty acids are inefficiently metabolized by the remnant liver, and infiltrate parenchyma, resulting in diffuse hepatocellular steatosis and, in some instances, to cell death [70–72]. This peculiar post-resection injury has been shown to peak between days 1 and 2 after 70%Hx, while it resolves and disppears thereafter in surviving rats. The RNAseq performed on day-1 liver samples showed that roxadustat tilts the balance of cellular functions, favoring lipid metabolism rather than cell replication, exactly by the moment of the worst lipid overload. Whether such a shift streamlines the postoperative recovery has to be ascertained. Still, Vic et al. previously proved that relieving steatosis via testosterone administration raised rat survival rate after 90% hepatectomy [71]. In set of additional experiences, we evaluated whether the level of intrahepatic or circulating portal and peripheral lipids might contribute to the explanation of our findings but the results of these extra measurements did not show differences between 70%Hx-RXD25 and 70%-placebo groups (Supplementary Information S6).

The improvement in cellular stress obtained after roxadustat treatment was an unforeseen finding and it may pave the way for the exploration of the role of selective HIF1α stabilization after liver resection. In other experimental settings, Roxadustat has shown to alleviate liver fatty infiltration in two zebrafish atp7b deficiency models of human Wilson's disease [73]. Since, in our surgical model, transient steatosis tends to physiologically vanish in surviving rats after d2, we could not expect to find a statistically significant difference after this time point, and we decided to discontinue the experiment on the grounds of ethical considerations.

© 2021 The Author(s). Published by Portland Press Limited on behalf of the Biochemical Society

Downloaded from http://portlandpress.com/clinsci/article-pdf/135/19/2285/921840/cs-2021-0183.pdf by Universita degli Studi di Milano user on 18 October 2021

It remains to be established whether isoquinolines are a treatment for fatty liver infiltration at large thanks to their action on steatosis and ballooning. Nonetheless the effect of roxadustat on steatosis and ballooning looks promising for the constellation of non-alcoholic fatty liver disease and steatohepatitis, whose incidence is alarmingly soaring in the general population. These conditions are known to be associated with defective liver regeneration after resection and with increased rate of primary non-function after transplantation if steatotic livers are used as grafts. The mechanism by which roxadustat might prompt the liver to process lipids is elucidated by the RNAseq analysis: a selective HIF1α stabilization largely elicited the transcription of genes coding for lipid metabolism and oxidative phosphorylation. What is more elusive is the possible significance of this effect in the context of hypoxia. Anaerobic metabolism is usually preferred in conditions of hypoxia [26,74], and, in fact, PHDs deletion [75–77] and vHL loss [78–80] originate the classical cellular response to hypoxia: decreased mitochondrial activity, increased glycolysis, and glycogen and lipid accumulation. However, increased cellular respiration results in a positive energy balance, a prerequisite for an improved liver function during regeneration. While not manifested by indicator other than decreased cell stress and ballooning in a paraphysiological standard 70%Hx, the exploration of roxadustat in hepatic surgery on steatotic livers is an intriguing perspective.

In conclusion, it remains unproven whether a roxadustat-induced selective HIF stabilization enhances function or proliferation during the early postoperative period after standard hepatectomy, when hypoxia responses are at their acme. However, roxadustat improved hepatocellular ballooning and fatty infiltration, signs of hepatocellular suffering and metabolic dysfunction, and this finding claims for further investigation of roxadustat in fatty liver diseases and of the role of hypoxia-simulating treatments after liver resection.

Clinical perspectives

- Hypoxia triggers liver regeneration after resection but it is controversial to actively induce hypoxia in patients undergoing hepatectomy. However, a hypoxic response can be simulated by means of roxadustat, a selective prolyl hydroxylase inhibitor that artificially stabilizes hypoxia inducible factor-1α (HIF1α) levels.
- The present study showed the administration of roxadustat concomitant with liver resection alleviated postoperative steatosis and ballooning, two hallmarks of liver suffering after resection, by raising HIF1α and increasing oxidative phosphorylation.
- Selective HIF stabilization does not accelerate liver regeneration but promotes cellular respiration and mitigate steatosis, suggesting a possible role for roxadustat in the surgery of steatotic livers and in the treatment of fatty liver disease at large.

Data Availability

The data that support the findings of the present study are available from the corresponding author, upon reasonable request. The RNAseq data will be freely available from https://www.ncbi.nlm.nih.gov/sra, under the BioProject ID: PRJNA705692.

Competing Interests

The authors declare that there are no competing interests associated with the manuscript.

Funding

The main researcher received an allowance from the Université catholique de Louvain [grant number ARH/LJB/1493-1133812].

CRediT Author Contribution

Samuele Iesari: Conceptualization, Data curation, Formal analysis, Validation, Investigation, Methodology, Writing—original draft, Writing—review & editing. **Isabelle Leclercq:** Conceptualization, Supervision, Methodology, Writing—original draft, Writing—review & editing. **Nicolas Joudiou:** Data curation, Investigation, Writing—review & editing. **Mina Komuta:** Data curation, Formal analysis, Writing—original draft, Writing—review & editing. **Aurélie Daumerie:** Data curation, Investigation, Writing—review & editing. **Jérôme Ambroise:** Software, Formal analysis, Writing—review & editing. **Alexandra Dili:** Conceptualization, Methodology, Writing—review & editing. **Natacha Feza-Bingi:** Investigation, Methodology, Writing—review &

Downloaded from http://portlandpress.com/clinsci/article-pdf/135/19/2285/921840/cs-2021-0183.pdf by Universita degli Studi di Milano user on 18 October 2021

© 2021 The Author(s). Published by Portland Press Limited on behalf of the Biochemical Society

Clinical Science (2021) **135** 2285–2305
https://doi.org/10.1042/CS20210183

editing. **Daela Xhema:** Investigation, Methodology, Writing—review & editing. **Caroline Bouzin:** Data curation, Investigation, Writing—review & editing. **Bernard Gallez:** Conceptualization, Methodology, Writing—review & editing. **Francesco Pisani:** Supervision, Validation, Project administration, Writing—review & editing. **Eliano Bonaccorsi-Riani:** Supervision, Validation, Methodology, Writing—review & editing. **Pierre Gianello:** Conceptualization, Resources, Supervision, Funding acquisition, Validation, Methodology, Project administration, Writing—review & editing.

Acknowledgements

We thank Gwen Beaurin, Guillaume Courtoy, Maxime De Rudder, Sébastien Druart, Boris Pirlot, Joachim Ravau, and Martial Vergauwen, for their precious technical support. We thank Álvaro Cortés Calabuig, Genomics Core Leuven, for his work with RNAseq. We thank Marta Fiorenza, English language lecturer, for her kind linguistic revision.

Abbreviations

AGPT2, angiopoietin-2; ALPPS, associating liver partition and portal vein ligation technique for two-stage hepatectomy; ALT, alanine aminotransferase; AST, aspartate aminotransferase; AUC, area under the curve; DMOG, dimethyloxalylglycine; DMSO, dimethyl sulfoxide; EDHB, ethyl-3,4-dihydroxybenzoate; EdU, 5-ethynyl-2′-deoxyuridine; Gd-EOB-DTPA, gadolinium ethoxybenzyl diethylenetriamine pentaacetic acid; GO, gene ontology; GSEA, gene set enrichment analysis; HDL, high-density lipoprotein; HIF, hypoxia-inducible factor; MRI, magnetic resonance imaging; OATP, organic anion-transporting polypeptide; ORA, over-representation analysis; PBS, phosphate-buffered saline; PHD, prolyl hydroxylase domain protein; RLBWR, remnant-liver-to-body-weight ratio; RNAseq, RNA sequencing; ROI, region of interest; RT-qPCR, real-time quantitative polymerase chain reaction; RXD, roxadustat; SFSS, small-for-size syndrome; 70%Hx, 70% hepatectomy.

References

1 Rahbari, N.N., Garden, O.J., Padbury, R. et al. (2011) Posthepatectomy liver failure: a definition and grading by the International Study Group of Liver Surgery (ISGLS). *Surgery* **149**, 713–724, https://doi.org/10.1016/j.surg.2010.10.001
2 Schadde, E., Tsatsaris, C., Swiderska-Syn, M. et al. (2017) Hypoxia of the growing liver accelerates regeneration. *Surgery* **161**, 666–679, https://doi.org/10.1016/j.surg.2016.05.018
3 Dili, A., Lebrun, V., Bertrand, C. and Leclercq, I.A. (2019) Associating liver partition and portal vein ligation for staged hepatectomy: establishment of an animal model with insufficient liver remnant. *Lab. Invest.* **99**, 698–707, https://doi.org/10.1038/s41374-018-0155-z
4 Dili, A., Bertrand, C., Lebrun, V., Pirlot, B. and Leclercq, I.A. (2019) Hypoxia protects the liver from Small For Size Syndrome: A lesson learned from the associated liver partition and portal vein ligation for staged hepatectomy (ALPPS) procedure in rats. *Am. J. Transplant.* **19**, 2979–2990, https://doi.org/10.1111/ajt.15420
5 Kron, P., Linecker, M., Limani, P. et al. (2016) Hypoxia-driven Hif2a coordinates mouse liver regeneration by coupling parenchymal growth to vascular expansion. *Hepatology* **64**, 2198–2209, https://doi.org/10.1002/hep.28809
6 Harnoss, J.M., Strowitzki, M.J., Radhakrishnan, P. et al. (2015) Therapeutic inhibition of prolyl hydroxylase domain-containing enzymes in surgery: putative applications and challenges. *Hypoxia (Auckl.)* **3**, 1–14
7 Schrock, T.R. and Hunt, T.K. (1972) Effect of respiratory hypoxia on hepatic regeneration. *Surg. Forum* **23**, 356–357
8 Campbell, W.L., Sheng, R., Zajko, A.B. et al. (1994) Intrahepatic biliary strictures after liver transplantation. *Radiology* **191**, 735–740, https://doi.org/10.1148/radiology.191.3.8184054
9 Harnoss, J.M., Platzer, L.K., Burhenne, J. et al. (2017) Prolyl hydroxylase inhibition enhances liver regeneration without induction of tumor growth. *Ann. Surg.* **265**, 782–791, https://doi.org/10.1097/SLA.0000000000001696
10 Duscher, D., Januszyk, M., Maan, Z.N. et al. (2017) Comparison of the hydroxylase inhibitor dimethyloxalylglycine and the iron chelator deferoxamine in diabetic and aged wound healing. *Plast. Reconstr. Surg.* **139**, 695e–706e, https://doi.org/10.1097/PRS.0000000000003072
11 Dirscherl, K., Schadde, E., Roth Z'Graggen, B. et al. (2018) The prolyl hydroxylase inhibitor DMOG inhibits hepatocyte proliferation, but induces growth of non-parenchymal cells in a rat model in vivo and in vitro, in 'Abstracts of Posters presented at the International Anesthesia Research Society 2018 Annual Meeting and International Science Symposium'. *Anesth. Analg.* **126**, 309
12 Trogadas, G., Mastoraki, A., Nastos, C. et al. (2015) Comparative effects of ischemic preconditioning and iron chelation in hepatectomy. *J. Invest. Surg.* **28**, 261–267, https://doi.org/10.3109/08941939.2015.1024803
13 Kyriazi, M.A., Theodoraki, K., Theodosopoulos, T. et al. (2011) Evaluation of ischemia-reperfusion liver injury by near-infrared spectroscopy in an experimental swine model: the effect of desferoxamine. *J. Invest. Surg.* **24**, 164–170, https://doi.org/10.3109/08941939.2011.560998
14 Nastos, C., Kalimeris, K., Papoutsidakis, N. et al. (2011) Antioxidant treatment attenuates intestinal mucosal damage and gut barrier dysfunction after major hepatectomy. Study in a porcine model. *J. Gastrointest. Surg.* **15**, 809–817, https://doi.org/10.1007/s11605-011-1475-0
15 Kalimeris, K., Nastos, C., Papoutsidakis, N. et al. (2010) Iron chelation prevents lung injury after major hepatectomy. *Hepatol. Res.* **40**, 841–850, https://doi.org/10.1111/j.1872-034X.2010.00682.x
16 Nastos, C., Contis, J., Kalimeris, K. et al. (2010) Antioxidant treatment attenuates hepatic encephalopathy after major hepatectomy in pigs, in 'Abstracts of the 16th Annual International Congress of the International Liver Transplantation Society. June 16-19, 2010. Hong Kong, China'. *Liver Transplant.* **16**, S69–S263

© 2021 The Author(s). Published by Portland Press Limited on behalf of the Biochemical Society

Downloaded from http://portlandpress.com/clinsci/article-pdf/135/19/2285/921840/cs-2021-0183.pdf by Universita degli Studi di Milano user on 18 October 2021

17 Arkadopoulos, N., Nastos, C., Kalimeris, K. et al. (2010) Iron chelation for amelioration of liver ischemia-reperfusion injury. *Hemoglobin* **34**, 265–277, https://doi.org/10.3109/03630269.2010.484766
18 Vollmar, B. and Menger, M.D. (2009) The hepatic microcirculation: mechanistic contributions and therapeutic targets in liver injury and repair. *Physiol. Rev.* **89**, 1269–1339, https://doi.org/10.1152/physrev.00027.2008
19 Abu-Amara, M., Gurusamy, K.S., Hori, S. et al. (2009) Pharmacological interventions versus no pharmacological intervention for ischaemia reperfusion injury in liver resection surgery performed under vascular control. *Cochrane Database Syst. Rev.* **4**, CD007472, https://doi.org/10.1002/14651858.CD007472.pub2
20 Fan, L., Li, J., Yu, Z. et al. (2014) The hypoxia-inducible factor pathway, prolyl hydroxylase domain protein inhibitors, and their roles in bone repair and regeneration. *Biomed Res. Int.* **2014**, 239356, https://doi.org/10.1155/2014/239356
21 Philipp, S., Cui, L., Ludolph, B. et al. (2006) Desferoxamine and ethyl-3,4-dihydroxybenzoate protect myocardium by activating NOS and generating mitochondrial ROS. *Am. J. Physiol. Heart Circ. Physiol.* **290**, H450–H457, https://doi.org/10.1152/ajpheart.00472.2005
22 Shen, X., Wan, C., Ramaswamy, G. et al. (2009) Prolyl hydroxylase inhibitors increase neoangiogenesis and callus formation following femur fracture in mice. *J. Orthop. Res.* **27**, 1298–1305, https://doi.org/10.1002/jor.20886
23 http://www.drugbank.ca/drugs/DB04847
24 Hoppe, G., Yoon, S., Gopalan, B. et al. (2016) Comparative systems pharmacology of HIF stabilization in the prevention of retinopathy of prematurity. *Proc. Natl. Acad. Sci. U.S.A.* **113**, E2516–E2525, https://doi.org/10.1073/pnas.1523005113
25 Beck, J., Henschel, C., Chou, J. et al. (2017) Evaluation of the carcinogenic potential of roxadustat (FG-4592), a small molecule inhibitor of hypoxia-inducible factor prolyl hydroxylase in CD-1 mice and Sprague Dawley rats. *Int. J. Toxicol.* **36**, 427–439, https://doi.org/10.1177/1091581817737232
26 Zhang, X., Liu, Z., Xiao, Q. et al. (2018) Donor treatment with a hypoxia-inducible factor-1 agonist prevents donation after cardiac death liver graft injury in a rat isolated perfusion model. *Artif. Organs* **42**, 280–289, https://doi.org/10.1111/aor.13005
27 Zhu, Y., Wang, Y., Jia, Y. et al. (2019) Roxadustat promotes angiogenesis through HIF-1α/VEGF/VEGFR2 signaling and accelerates cutaneous wound healing in diabetic rats. *Wound Repair Regen.* **27**, 324–334, https://doi.org/10.1111/wrr.12708
28 Emond, J., Capron-Laudereau, M., Meriggi, F. et al. (1989) Extent of hepatectomy in the rat. Evaluation of basal conditions and effect of therapy. *Eur. Surg. Res.* **21**, 251–259, https://doi.org/10.1159/000129034
29 Higgins, G. and Anderson, R. (1931) Experimental pathology of the liver. *Arch. Pathol.* **12**, 186–202
30 Kubota, T., Takabe, K., Yang, M. et al. (1997) Minimum sizes for remnant and transplanted livers in rats. *J. Hepatobiliary Pancreat. Surg.* **4**, 398–404, https://doi.org/10.1007/BF02488972
31 Katsube, T., Okada, M., Kumano, S. et al. (2011) Estimation of liver function using T1 mapping on Gd-EOB-DTPA-enhanced magnetic resonance imaging. *Invest. Radiol.* **46**, 277–283, https://doi.org/10.1097/RLI.0b013e318200f67d
32 Ünal, E., Akata, D. and Karcaaltincaba, M. (2016) Liver function assessment by magnetic resonance imaging. *Semin. Ultrasound CT MR* **37**, 549–560, https://doi.org/10.1053/j.sult.2016.08.006
33 Yoshikawa, K., Inoue, Y., Akahane, M. et al. (2003) Phantom and animal studies of a new hepatobiliary agent for MR imaging: comparison of Gd-DTPA-DeA with Gd-EOB-DTPA. *J. Magn. Reson. Imaging* **18**, 204–209, https://doi.org/10.1002/jmri.10349
34 Motosugi, U., Ichikawa, T., Sou, H. et al. (2009) Liver parenchymal enhancement of hepatocyte-phase images in Gd-EOB-DTPA-enhanced MR imaging: which biological markers of the liver function affect the enhancement? *J. Magn. Reson. Imaging* **30**, 1042–1046, https://doi.org/10.1002/jmri.21956
35 Ma, C., Liu, A., Wang, Y. et al. (2014) The hepatocyte phase of Gd-EOB-DTPA-enhanced MRI in the evaluation of hepatic fibrosis and early liver cirrhosis in a rat model: an experimental study. *Life Sci.* **108**, 104–108, https://doi.org/10.1016/j.lfs.2014.05.016
36 Ulloa, J.L., Stahl, S., Yates, J. et al. (2013) Assessment of gadoxetate DCE-MRI as a biomarker of hepatobiliary transporter inhibition. *NMR Biomed.* **26**, 1258–1270, https://doi.org/10.1002/nbm.2946
37 Barnes, S.L., Whisenant, J.G., Loveless, M.E. and Yankeelov, T.E. (2012) Practical dynamic contrast enhanced MRI in small animal models of cancer: data acquisition, data analysis, and interpretation. *Pharmaceutics* **4**, 442–478, https://doi.org/10.3390/pharmaceutics4030442
38 Kietzmann, T. (2017) Metabolic zonation of the liver: the oxygen gradient revisited. *Redox Biol.* **11**, 622–630, https://doi.org/10.1016/j.redox.2017.01.012
39 Jack, E.M., Bentley, P., Bieri, F. et al. (1990) Increase in hepatocyte and nuclear volume and decrease in the population of binucleated cells in preneoplastic foci of rat liver: a stereological study using the nucleator method. *Hepatology* **11**, 286–297, https://doi.org/10.1002/hep.1840110220
40 Peters, R. (1984) Nucleo-cytoplasmic flux and intracellular mobility in single hepatocytes measured by fluorescence microphotolysis. *EMBO J.* **3**, 1831–1836, https://doi.org/10.1002/j.1460-2075.1984.tb02055.x
41 http://www.bioinformatics.babraham.ac.uk/projects/fastqc/
42 Aronesty, E. (2013) Comparison of sequencing utility programs. *Open Bioinform. J.* **7**, 1–8, https://doi.org/10.2174/1875036201307010001
43 https://github.com/ExpressionAnalysis/ea-utils
44 Li, H., Handsaker, B., Wysoker, A. et al. (2009) The Sequence Alignment/Map format and SAMtools. *Bioinformatics* **25**, 2078–2079, https://doi.org/10.1093/bioinformatics/btp352
45 Love, M.I., Huber, W. and Anders, S. (2014) Moderated estimation of fold change and dispersion for RNA-seq data with DESeq2. *Genome Biol.* **15**, 550, https://doi.org/10.1186/s13059-014-0550-8
46 Liao, Y., Wang, J., Jaehnig, E.J. et al. (2019) WebGestalt 2019: gene set analysis toolkit with revamped UIs and APIs. *Nucleic Acids Res.* **47**, W199–W205, https://doi.org/10.1093/nar/gkz401
47 Ashburner, M., Ball, C.A., Blake, J.A. et al. (2000) Gene ontology: tool for the unification of biology. The Gene Ontology Consortium. *Nat. Genet.* **25**, 25–29, https://doi.org/10.1038/75556

Downloaded from http://portlandpress.com/clinsci/article-pdf/135/19/2285/921840/cs-2021-0183.pdf by Universita degli Studi di Milano user on 18 October 2021

© 2021 The Author(s). Published by Portland Press Limited on behalf of the Biochemical Society

48 The Gene Ontology Consortium (2019) The Gene Ontology Resource: 20 years and still GOing strong. *Nucleic Acids Res.* **47**, D330–D338, https://doi.org/10.1093/nar/gky1055
49 Kanehisa, M. and Goto, S. (2000) KEGG: kyoto encyclopedia of genes and genomes. *Nucleic Acids Res.* **28**, 27–30, https://doi.org/10.1093/nar/28.1.27
50 Jassal, B., Matthews, L., Viteri, G. et al. (2020) The reactome pathway knowledgebase. *Nucleic Acids Res.* **48**, D498–D503
51 Mi, H., Muruganujan, A., Ebert, D. et al. (2018) PANTHER version 14: more genomes, a new PANTHER GO-slim and improvements in enrichment analysis tools. *Nucleic Acids Res.* **47**, D419–D426, https://doi.org/10.1093/nar/gky1038
52 Borger, P., Buzdin, A., Sorokin, M. et al. (2020) Large-scale profiling of signaling pathways reveals a distinct demarcation between normal and extended liver resection. *Cells* **9**, 1149, https://doi.org/10.3390/cells9051149
53 Qi, J., You, T., Pan, T. et al. (2017) Downregulation of hypoxia-inducible factor-1α contributes to impaired megakaryopoiesis in immune thrombocytopenia. *Thromb. Haemost.* **117**, 1875–1886, https://doi.org/10.1055/s-0039-1694030
54 Kim, J.Y., Choi, D., Kim, J. et al. (2020) Co-administration of erythropoietin and iron complex improves late-phase liver regeneration. *BMB Rep.* **53**, 148–153, https://doi.org/10.5483/BMBRep.2020.53.3.160
55 Suresh, S., Rajvanshi, P.K. and Noguchi, C.T. (2020) The many facets of erythropoietin physiologic and metabolic response. *Front. Physiol.* **10**, 1534, https://doi.org/10.3389/fphys.2019.01534
56 Schneider, M., Van Geyte, K., Fraisl, P. et al. (2010) Loss or silencing of the PHD1 prolyl hydroxylase protects livers of mice against ischemia/reperfusion injury. *Gastroenterology* **138**, 1143–1154.e1141-1142, https://doi.org/10.1053/j.gastro.2009.09.057
57 Fujita, N., Chiba, K., Shapiro, I.M. and Risbud, M.V. (2012) HIF-1α and HIF-2α degradation is differentially regulated in nucleus pulposus cells of the intervertebral disc. *J. Bone Miner. Res.* **27**, 401–412, https://doi.org/10.1002/jbmr.538
58 Tralhão, J.G., Abrantes, A.M., Hoti, E. et al. (2014) Hepatectomy and liver regeneration: from experimental research to clinical application. *ANZ J. Surg.* **84**, 665–671, https://doi.org/10.1111/ans.12201
59 Moris, D. and Pawlik, T.M. (2017) Liver hypoxia as a trigger to liver regeneration: no more than another piece of the puzzle. *Surgery* **161**, 1176–1177, https://doi.org/10.1016/j.surg.2016.08.051
60 Rahman, T.M. and Hodgson, H.J. (2000) Animal models of acute hepatic failure. *Int. J. Exp. Pathol.* **81**, 145–157, https://doi.org/10.1046/j.1365-2613.2000.00144.x
61 Ballatori, N., Hammond, C.L., Cunningham, J.B. et al. (2005) Molecular mechanisms of reduced glutathione transport: role of the MRP/CFTR/ABCC and OATP/SLC21A families of membrane proteins. *Toxicol. Appl. Pharmacol.* **204**, 238–255, https://doi.org/10.1016/j.taap.2004.09.008
62 Bakos, E., Hegedüs, T., Holló, Z. et al. (1996) Membrane topology and glycosylation of the human multidrug resistance-associated protein. *J. Biol. Chem.* **271**, 12322–12326, https://doi.org/10.1074/jbc.271.21.12322
63 Leonhardt, M., Keiser, M., Oswald, S. et al. (2010) Hepatic uptake of the magnetic resonance imaging contrast agent Gd-EOB-DTPA: role of human organic anion transporters. *Drug Metab. Dispos.* **38**, 1024–1028, https://doi.org/10.1124/dmd.110.032862
64 You, M.-W., Kim, H.J., Lim, H.-S. et al. (2018) Assessment of liver function using pharmacokinetic parameters of Gd-EOB-DTPA: experimental study in rat hepatectomy model. *Contrast Media Mol. Imaging* **2018**, 6321316, https://doi.org/10.1155/2018/6321316
65 Article 3, paragraph 3 of the Directive 2010/63/EU. (http://data.europa.eu/eli/dir/2010/63/oj)
66 Rahman, T.M. and Hodgson, H.J.F. (2000) Animal models of acute hepatic failure. *Int. J. Exp. Pathol.* **81**, 145–157, https://doi.org/10.1046/j.1365-2613.2000.00144.x
67 Moris, D. and Schadde, E. (2017) It is the function of regenerating liver parenchyma that explains the small for size syndrome. *J. Surg. Res.* **217**, 237, https://doi.org/10.1016/j.jss.2017.02.076
68 Michalopoulos, G.K. (2017) Hepatostat: liver regeneration and normal liver tissue maintenance. *Hepatology* **65**, 1384–1392, https://doi.org/10.1002/hep.28988
69 Mollenhauer, M., Kiss, J., Dudda, J. et al. (2012) Deficiency of the oxygen sensor PHD1 augments liver regeneration after partial hepatectomy. *Langenbecks Arch. Surg.* **397**, 1313–1322, https://doi.org/10.1007/s00423-012-0998-5
70 Bengmark, S. (1969) Liver steatosis and liver resection. *Digestion* **2**, 304–311, https://doi.org/10.1159/000196955
71 Vic, P., Saint-Aubert, B., Astre, C. et al. (1982) Complete liver regeneration in one-stage 90% hepatectomized rats treated with testosterone. *Hepatology* **2**, 247–248, https://doi.org/10.1002/hep.1840020210
72 Bucher, N.L. (1963) Regeneration of mammalian liver. *Int. Rev. Cytol.* **15**, 245–300, https://doi.org/10.1016/S0074-7696(08)61119-5
73 Mi, X., Li, Z., Yan, J. et al. (2020) Activation of HIF-1 signaling ameliorates liver steatosis in zebrafish atp7b deficiency (Wilson's disease) models. *Biochim. Biophys. Acta Mol. Basis Dis.* **1866**, 165842, https://doi.org/10.1016/j.bbadis.2020.165842
74 Frezza, C., Zheng, L., Tennant, D.A. et al. (2011) Metabolic profiling of hypoxic cells revealed a catabolic signature required for cell survival. *PLoS ONE* **6**, e24411, https://doi.org/10.1371/journal.pone.0024411
75 Aragonés, J., Schneider, M., Van Geyte, K. et al. (2008) Deficiency or inhibition of oxygen sensor Phd1 induces hypoxia tolerance by reprogramming basal metabolism. *Nat. Genet.* **40**, 170–180, https://doi.org/10.1038/ng.2007.62
76 Minamishima, Y.A., Moslehi, J., Padera, R.F. et al. (2009) A feedback loop involving the Phd3 prolyl hydroxylase tunes the mammalian hypoxic response in vivo. *Mol. Cell. Biol.* **29**, 5729–5741, https://doi.org/10.1128/MCB.00331-09
77 Duan, L.-J., Takeda, K. and Fong, G.-H. (2014) Hematological, hepatic, and retinal phenotypes in mice deficient for prolyl hydroxylase domain proteins in the liver. *Am. J. Pathol.* **184**, 1240–1250, https://doi.org/10.1016/j.ajpath.2013.12.014
78 Hervouet, E., Demont, J., Pecina, P. et al. (2005) A new role for the von Hippel-Lindau tumor suppressor protein: stimulation of mitochondrial oxidative phosphorylation complex biogenesis. *Carcinogenesis* **26**, 531–539, https://doi.org/10.1093/carcin/bgi001
79 Wise, D.R., Ward, P.S., Shay, J.E.S. et al. (2011) Hypoxia promotes isocitrate dehydrogenase-dependent carboxylation of α-ketoglutarate to citrate to support cell growth and viability. *Proc. Natl. Acad. Sci. U.S.A.* **108**, 19611, https://doi.org/10.1073/pnas.1117773108

Downloaded from http://portlandpress.com/clinsci/article-pdf/135/19/2285/921840/cs-2021-0183.pdf by Universita degli Studi di Milano user on 18 October 2021

© 2021 The Author(s). Published by Portland Press Limited on behalf of the Biochemical Society

80 Zhang, H., Gao, P., Fukuda, R. et al. (2007) HIF-1 inhibits mitochondrial biogenesis and cellular respiration in vhl-deficient renal cell carcinoma by repression of C-MYC activity. *Cancer Cell* **11**, 407–420, https://doi.org/10.1016/j.ccr.2007.04.001

81 Subramanian, A., Tamayo, P., Mootha, V.K. et al. (2005) Gene set enrichment analysis: a knowledge-based approach for interpreting genome-wide expression profiles. *Proc. Natl. Acad. Sci. U.S.f.* **102**, 15545–15550, https://doi.org/10.1073/pnas.0506580102

Downloaded from http://portlandpress.com/clinsci/article-pdf/135/19/2285/921840/cs-2021-0183.pdf by Universita degli Studi di Milano user on 18 October 2021

© 2021 The Author(s). Published by Portland Press Limited on behalf of the Biochemical Society